Trapp, B. D., Peterson, J., Ransohoff, R. M., Rudick, R., Mork, S., and Bo, L. (1998). Axonal transection in the lesions of multiple sclerosis. *N. Engl. J. Med.* 338, 278–285. doi: 10.1056/NEJM199801293380502

Tsacopoulos, M., and Magistretti, P. J. (1996). Metabolic coupling between glia and neurons. *J. Neurosci.* 16, 877–885.

Umebayashi, D., Natsume, A., Takeuchi, H., Hara, M., Nishimura, Y., Fukuyama, R., et al. (2014). Blockade of gap junction hemichannel protects secondary spinal cord injury from activated microglia-mediated glutamate exitoneurotoxicity. *J. Neurotrauma.* doi: 10.1089/neu.2013.3223. [Epub ahead of print].

Upender, M. B., and Naegele, J. R. (1999). Activation of microglia during developmentally regulated cell death in the cerebral cortex. *Dev. Neurosci.* 21, 491–505. doi: 10.1159/000017416

Valcour, V., Sithinamsuwan, P., Letendre, S., and Ances, B. (2011). Pathogenesis of HIV in the central nervous system. *Curr. HIV/AIDS Rep.* 8, 54–61. doi: 10.1007/s11904-010-0070-4

Valiunas, V., Polosina, Y. Y., Miller, H., Potapova, I. A., Valiuniene, L., Doronin, S., et al. (2005). Connexin-specific cell-to-cell transfer of short interfering RNA by gap junctions. *J. Physiol.* 568, 459–468. doi: 10.1113/jphysiol.2005.090985

Wallraff, A., Kohling, R., Heinemann, U., Theis, M., Willecke, K., and Steinhauser, C. (2006). The impact of astrocytic gap junctional coupling on potassium buffering in the hippocampus. *J. Neurosci.* 26, 5438–5447. doi: 10.1523/JNEUROSCI.0037-06.2006

Wallraff, A., Odermatt, B., Willecke, K., and Steinhauser, C. (2004). Distinct types of astroglial cells in the hippocampus differ in gap junction coupling. *Glia* 48, 36–43. doi: 10.1002/glia.20040

Walz, W., and Hertz, L. (1983). Functional interactions between neurons and astrocytes. II. Potassium homeostasis at the cellular level. *Prog. Neurobiol.* 20, 133–183. doi: 10.1016/0301-0082(83)90013-8

Wang, J., Ma, M., Locovei, S., Keane, R. W., and Dahl, G. (2007). Modulation of membrane channel currents by gap junction protein mimetic peptides: size matters. *Am. J. Physiol. Cell Physiol.* 293, C1112–C1119. doi: 10.1152/ajpcell.00097.2007

Wasseff, S. K., and Scherer, S. S. (2014). Activated microglia do not form functional gap junctions *in vivo*. *J. Neuroimmunol.* 269, 90–93. doi: 10.1016/j.jneuroim.2014.02.005

Willecke, K., Eiberger, J., Degen, J., Eckardt, D., Romualdi, A., Guldenagel, M., et al. (2002). Structural and functional diversity of connexin genes in the mouse and human genome. *Biol. Chem.* 383, 725–737. doi: 10.1515/BC.2002.076

Wong, R. O., Chernjavsky, A., Smith, S. J., and Shatz, C. J. (1995). Early functional neural networks in the developing retina. *Nature* 374, 716–718. doi: 10.1038/374716a0

Wu, D. C., Jackson-Lewis, V., Vila, M., Tieu, K., Teismann, P., Vadseth, C., et al. (2002). Blockade of microglial activation is neuroprotective in the 1-methyl-4-phenyl-1,2,3,6-tetrahydropyridine mouse model of Parkinson disease. *J. Neurosci.* 22, 1763–1771.

Wu, Z., Tokuda, Y., Zhang, X. W., and Nakanishi, H. (2008). Age-dependent responses of glial cells and leptomeninges during systemic inflammation. *Neurobiol. Dis.* 32, 543–551. doi: 10.1016/j.nbd.2008.09.002

Xiong, J., and Kielian, T. (2013). Microglia in juvenile neuronal ceroid lipofuscinosis are primed toward a pro-inflammatory phenotype. *J. Neurochem.* 127, 245–258. doi: 10.1111/jnc.12385

Xu, Q., Cheong, Y. K., He, S. Q., Tiwari, V., Liu, J., Wang, Y., et al. (2014). Suppression of spinal connexin 43 expression attenuates mechanical hypersensitivity in rats after an L5 spinal nerve injury. *Neurosci. Lett.* 566, 194–199. doi: 10.1016/j.neulet.2014.03.004

Xu, X., Li, W. E., Huang, G. Y., Meyer, R., Chen, T., Luo, Y., et al. (2001). Modulation of mouse neural crest cell motility by N-cadherin and connexin 43 gap junctions. *J. Cell Biol.* 154, 217–230. doi: 10.1083/jcb.200105047

Yamanaka, K., Chun, S. J., Boillee, S., Fujimori-Tonou, N., Yamashita, H., Gutmann, D. H., et al. (2008). Astrocytes as determinants of disease progression in inherited amyotrophic lateral sclerosis. *Nat. Neurosci.* 11, 251–253. doi: 10.1038/nn2047

Yawata, I., Takeuchi, H., Doi, Y., Liang, J., Mizuno, T., and Suzumura, A. (2008). Macrophage-induced neurotoxicity is mediated by glutamate and attenuated by glutaminase inhibitors and gap junction inhibitors. *Life Sci.* 82, 1111–1116. doi: 10.1016/j.lfs.2008.03.010

Ye, Z. C., Wyeth, M. S., Baltan-Tekkok, S., and Ransom, B. R. (2003). Functional hemichannels in astrocytes: a novel mechanism of glutamate release. *J. Neurosci.* 23, 3588–3596.

Yeager, M., and Harris, A. L. (2007). Gap junction channel structure in the early 21st century: facts and fantasies. *Curr. Opin. Cell Biol.* 19, 521–528. doi: 10.1016/j.ceb.2007.09.001

Yrjanheikki, J., Keinanen, R., Pellikka, M., Hokfelt, T., and Koistinaho, J. (1998). Tetracyclines inhibit microglial activation and are neuroprotective in global brain ischemia. *Proc. Natl. Acad. Sci. U.S.A.* 95, 15769–15774. doi: 10.1073/pnas.95.26.15769

Yudkoff, M. (1997). Brain metabolism of branched-chain amino acids. *Glia* 21, 92–98. doi: 10.1002/(SICI)1098-1136(199709)21:1<92::AID-GLIA10>3.0.CO;2-W

Zhu, S., Stavrovskaya, I. G., Drozda, M., Kim, B. Y., Ona, V., Li, M., et al. (2002). Minocycline inhibits cytochrome c release and delays progression of amyotrophic lateral sclerosis in mice. *Nature* 417, 74–78. doi: 10.1038/417074a

Zietlow, R., Dunnett, S. B., and Fawcett, J. W. (1999). The effect of microglia on embryonic dopaminergic neuronal survival *in vitro*: diffusible signals from neurons and glia change microglia from neurotoxic to neuroprotective. *Eur. J. Neurosci.* 11, 1657–1667. doi: 10.1046/j.1460-9568.1999.00583.x

Ziv, Y., Avidan, H., Pluchino, S., Martino, G., and Schwartz, M. (2006a). Synergy between immune cells and adult neural stem/progenitor cells promotes functional recovery from spinal cord injury. *Proc. Natl. Acad. Sci. U.S.A.* 103, 13174–13179. doi: 10.1073/pnas.0603747103

Ziv, Y., Ron, N., Butovsky, O., Landa, G., Sudai, E., Greenberg, N., et al. (2006b). Immune cells contribute to the maintenance of neurogenesis and spatial learning abilities in adulthood. *Nat. Neurosci.* 9, 268–275. doi: 10.1038/nn1629

Zlomuzica, A., Reichinnek, S., Maxeiner, S., Both, M., May, E., Worsdorfer, P., et al. (2010). Deletion of connexin45 in mouse neurons disrupts one-trial object recognition and alters kainate-induced gamma-oscillations in the hippocampus. *Physiol. Behav.* 101, 245–253. doi: 10.1016/j.physbeh.2010.05.007

Conflict of Interest Statement: The authors declare that the research was conducted in the absence of any commercial or financial relationships that could be construed as a potential conflict of interest.

Received: 31 March 2014; paper pending published: 07 April 2014; accepted: 19 June 2014; published online: 02 September 2014.

Citation: Takeuchi H and Suzumura A (2014) Gap junctions and hemichannels composed of connexins: potential therapeutic targets for neurodegenerative diseases. Front. Cell. Neurosci. 8:189. doi: 10.3389/fncel.2014.00189

This article was submitted to the journal Frontiers in Cellular Neuroscience.

PLOS | ONE

Granulocyte-Colony Stimulating Factor Attenuates Oligomeric Amyloid β Neurotoxicity by Activation of Neprilysin

Yukiko Doi[1☯], Hideyuki Takeuchi[1☯], Hiroyuki Mizoguchi[2], Kazuya Fukumoto[2], Hiroshi Horiuchi[1], Shijie Jin[1], Jun Kawanokuchi[1], Bijay Parajuli[1], Yoshifumi Sonobe[1], Tetsuya Mizuno[1]*, Akio Suzumura[1]

1 Department of Neuroimmunology, Research Institute of Environmental Medicine, Nagoya University, Nagoya, Japan, **2** Futuristic Environmental Simulation Center, Research Institute of Environmental Medicine, Nagoya University, Nagoya, Japan

Abstract

Soluble oligomeric amyloid β (oAβ) causes synaptic dysfunction and neuronal cell death, which are involved in the pathogenesis of Alzheimer's disease (AD). The hematopoietic growth factor granulocyte-colony stimulating factor (G-CSF) is expressed in the central nervous system (CNS) and drives neurogenesis. Here we show that G-CSF attenuated oAβ neurotoxicity through the enhancement of the enzymatic activity of Aβ-degrading enzyme neprilysin (NEP) in neurons, while the NEP inhibitor thiorphan abolished the neuroprotection. Inhibition of MEK5/ERK5, a major downstream effector of G-CSF signaling, also ablated neuroprotective effect of G-CSF. Furthermore, intracerebroventricular administration of G-CSF enhanced NEP enzymatic activity and clearance of Aβ in APP/PS1 transgenic mice. Thus, we propose that G-CSF may be a possible therapeutic strategy against AD.

Citation: Doi Y, Takeuchi H, Mizoguchi H, Fukumoto K, Horiuchi H, et al. (2014) Granulocyte-Colony Stimulating Factor Attenuates Oligomeric Amyloid β Neurotoxicity by Activation of Neprilysin. PLoS ONE 9(7): e103458. doi:10.1371/journal.pone.0103458

Editor: Koichi M. Iijima, National Center for Geriatrics and Gerontology, Japan

Received March 23, 2014; **Accepted** June 29, 2014; **Published** July 25, 2014

Data Availability: The authors confirm that all data underlying the findings are fully available without restriction. All relevant data are within the paper and its Supporting Information files.

Funding: This work was supported in part by grants from the Ministry of Education, Culture, Sports, Science and Technology of Japan; a grant from the Advanced Research for Medical Products Mining Program of the National Institute of Biomedical Innovation (NIBIO) of Japan; and grants from the Ministry of Health, Labour and Welfare of Japan. The funders had no role in study design, data collection and analysis, decision to publish, or preparation of the manuscript.

Competing Interests: The authors have declared that no competing interests exist.

* Email: tmizuno@riem.nagoya-u.ac.jp

☯ These authors contributed equally to this work.

Introduction

Alzheimer's disease (AD) is a neurodegenerative disorder and the most common cause of dementia in the elderly. One of the pathological hallmarks of AD is senile plaque, whose major component is fibrillar amyloid β (fAβ). While fAβ-induces neuronal dystrophy and tau hyperphosphorylation [1,2], soluble oligomeric Aβ (oAβ) has been reported to exhibit higher neurotoxicity than fAβ. oAβ reportedly inhibits hippocampal long-term potentiation and disrupts synaptic plasticity [3,4].

Granulocyte-colony stimulating factor (G-CSF) is a major growth factor in the differentiation and proliferation of neutrophilic-granulocytic lineage cells that modulates the immune response by inhibiting the production of inflammatory cytokines [5,6]. Both G-CSF and its receptor G-CSFR are widely expressed in neurons in the central nervous systems (CNS), and their expression is induced by ischemia [7]. G-CSFR is also reportedly expressed in adult neural stem cells, and G-CSF can induce neuronal differentiation *in vitro* [7]. However, the exact functions of G-CSF await further elucidation.

Administration of G-CSF has been shown to improve cognitive performance in an AD model mouse carrying the Tg2576 transgene without reduction of Aβ burden [8]. The mechanism is reported to be due to local neurogenesis surrounding Aβ aggregates and the enhancement of acetylcholine levels. Another report shows that G-CSF ameliorates cognitive impairments with accompanying decreases of Aβ burden in APP/PS1 transgenic (Tg) mouse model of AD [9]. The study reported that the effects of G-CSF are due to upregulation of neurogenesis by neuronal stem cells and Aβ clearance by microglia. However, the precise functions of G-CSF on mature neurons are not fully understood. Increasing zinc-metalloprotease neprilysin (NEP) activity in AD mouse models reportedly improves cognitive impairments [10]. Indeed, NEP is one of the most prominent Aβ degrading enzymes. In this study, we show that G-CSF attenuates $oA\beta_{1-42}$ toxicity via activation of NEP.

Materials and Methods

Preparation of oligomeric $A\beta_{1-42}$

Soluble oligomeric amyloid β_{1-42} ($oA\beta_{1-42}$) was prepared as described previously [11]. Briefly, synthetic human $A\beta_{1-42}$ (Peptide Institute, Osaka, Japan) was dissolved in 100% 1,1,1,3,3,3-hexafluoro-2-propanol at a concentration of 1 mM. This solution was completely dried by the vacuum desiccator. The obtained film was resuspended in dimethyl sulfoxide to a concentration of 5 mM, and diluted with Dulbecco's Modified Eagle Medium/F12 (Invitrogen, Carlsbad, CA, USA) at a

concentration of 100 μM. This solution was incubated at 4°C for 24 h to obtain $oA\beta_{1-42}$. A final concentration of 5 μM $oA\beta_{1-42}$ was used in all experiments.

Animals

This study was carried out in strict accordance with the guideline for the care and use of laboratory animals of Nagoya University. All protocols for animal experiments were approved by the Animal Experiment Committee of Nagoya University. Transgenic mice expressing mutant variants of human amyloid precursor protein (APP) with K595N and M596L mutations and presenilin 1 (PS1) with A264E mutation were purchased from the Jackson Laboratory (B6C3-Tg(APP695)3Dbo Tg(PSEN1)5Dbo/J; #003378) and were backcrossed to C57BL/6J mice for more than 10 generations after purchase (here designated as APP/PS1 Tg mice).

G-CSF (30 ng/3 μl) or vehicle [phosphate-buffered saline (PBS)] was injected into the cerebral ventricular space of 12-month-old APP/PS1 Tg mice as previously described [12,13]. Three days after injection, deep-anesthetized mice were transcardially perfused with ice-cold PBS, and the brains were collected. The left hemispheres were used for histological analysis, and the right hemispheres were used for assessments of neprilysin enzymatic activity and Aβ concentration.

Neuronal culture

Primary mouse cortical neurons were prepared as previously described [11,14]. Briefly, cerebral cortices were isolated from C57BL/6J mouse embryos on the 17th embryonic day, minced

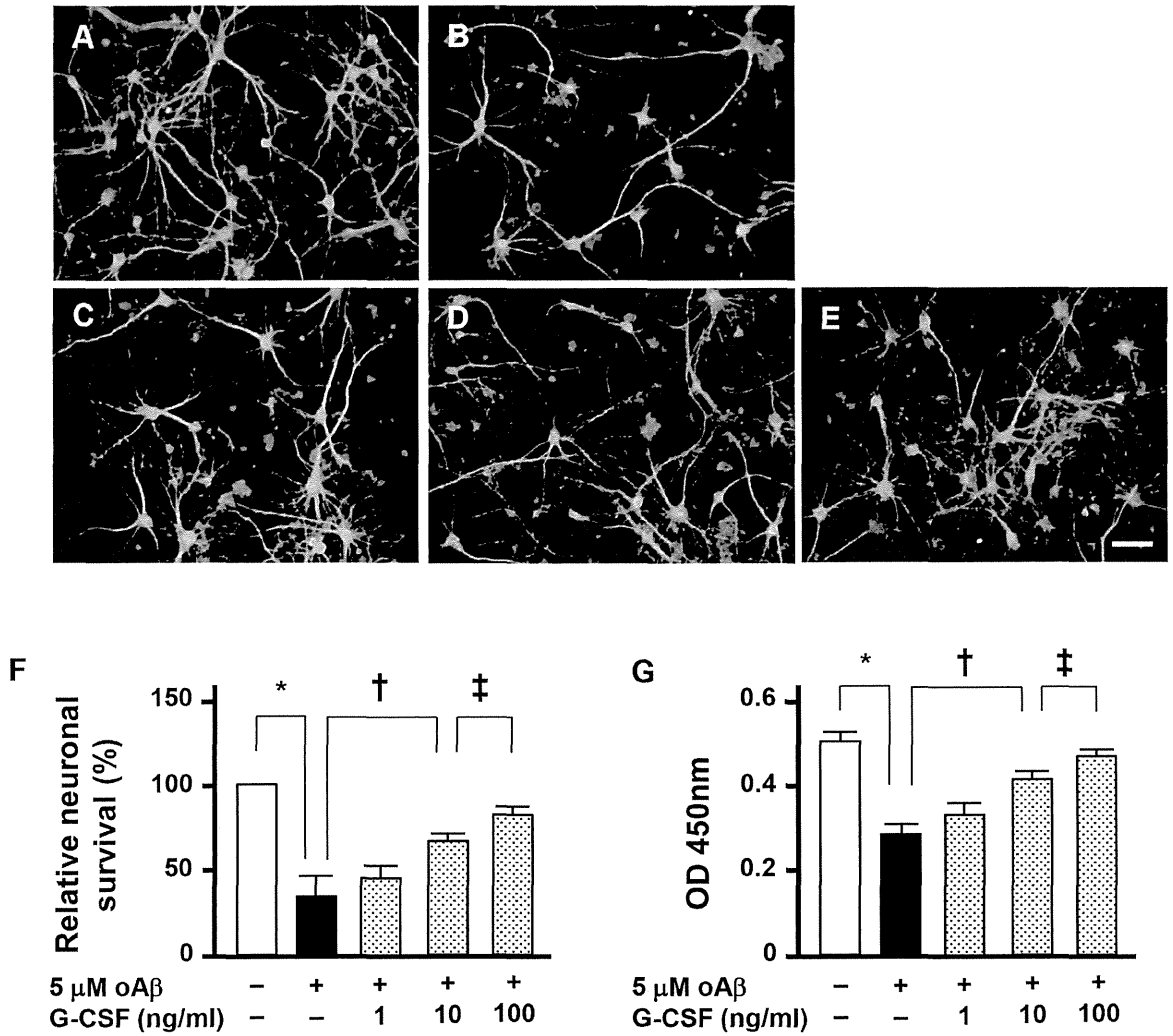

Figure 1. G-CSF suppresses oAβ-induced neurotoxicity. A–E, Fluorescent microscopic images of mouse primary cortical neuron cultures. A, Untreated neurons. B, Neurons treated with 5 μM $oA\beta_{1-42}$. C, Neurons treated with 5 μM $oA\beta_{1-42}$ and 1 ng/ml G-CSF. D, Neurons treated with 5 μM $oA\beta_{1-42}$ and 10 ng/ml G-CSF. E, Neurons treated with 5 μM $oA\beta_{1-42}$ and 100 ng/ml G-CSF. Treatment with G-CSF was neuroprotective against oAβ-mediated toxicity. Neurons were stained with anti-MAP-2 antibodies (green), and Aβ was stained with 4G8 antibodies (red). Scale bar: 50 μm. F, Relative neuronal survival. The number of viable neurons (MAP-2–positive neurons) was quantified relative to results observed with untreated neurons. G-CSF rescued neurons against oAβ-mediated toxicity in a dose-dependent manner. *, $p<0.001$; †, $p<0.01$; ††, $p<0.05$. Values are means ± SEM (n = 3). G, WST-8 assay. G-CSF enhanced neuronal survival against oAβ-mediated toxicity in a dose-dependent manner. *, $p<0.001$; †, $p<0.01$; ††, $p<0.05$. Values are means ± SEM (n = 6).
doi:10.1371/journal.pone.0103458.g001

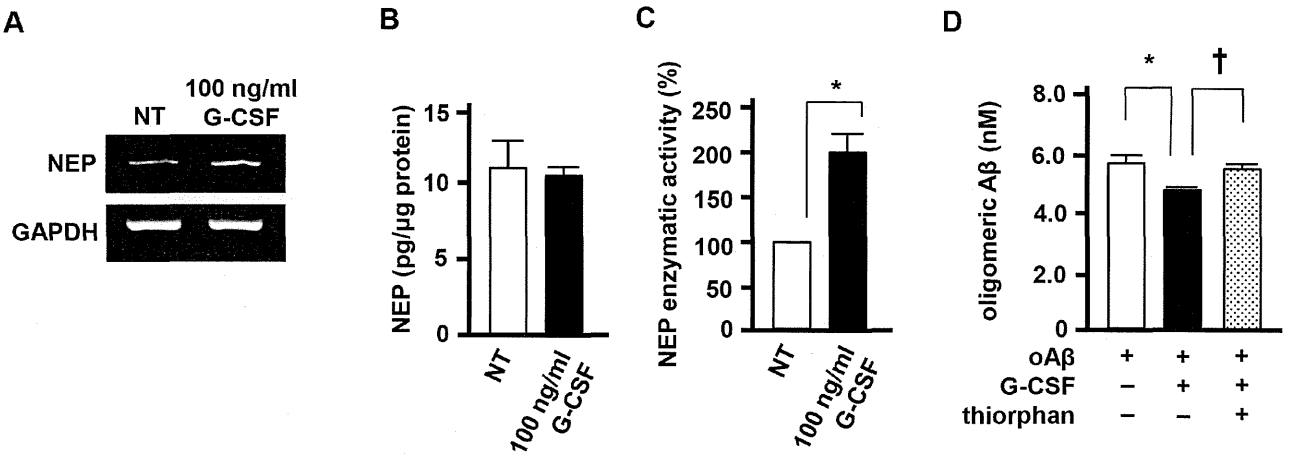

Figure 2. G-CSF enhances oAβ degradation by activation of NEP. A, Representative RT-PCR data for NEP in neurons. G-CSF stimulation upregulated NEP expression. NT, no treatment. B, ELISA data for NEP. NT, no treatment. Values are means ± SEM (n = 3). C, NEP enzymatic activity assay. G-CSF stimulation enhanced NEP enzymatic activity whereas NEP protein level was not affected. NT, no treatment. *, $p<0.05$. Values are means ± SEM (n = 3). D, ELISA data for oAβ. G-CSF treatment reduced the amount of $oA\beta_{1-42}$ in the supernatants of neuronal cultures, whereas the NEP inhibitor thiorphan ablated this effect. *, $p<0.01$; †, $p<0.05$. Values are means ± SEM (n = 3).
doi:10.1371/journal.pone.0103458.g002

and treated with dissociation solution (Sumitomo Bakelite, Akita, Japan). Neurons were resuspended in Nerve Culture Medium (Sumitomo Bakelite), plated on polyethylenimine-coated glass coverslips (Asahi Techno Glass, Chiba, Japan) at a density of 5×10^3 cells/well in 96-well multidishes, 5×10^4 cells/well in 24-well multidishes, or 6×10^6 cells/well in 6-well multidishes, and incubated at 37°C in an atmosphere containing 5% CO_2 at 100% humidity. The purity of the cultures was greater than 95% based on NeuN-specific immunostaining. Neurons were used at 14 days *in vitro* for the following assessments.

Immunocytochemistry

Neurons were plated at a density of 5×10^4 cells per well in 24-well multidishes, and stimulated with 1–100 ng/ml G-CSF (R&D Systems) 3 h before $oA\beta_{1-42}$ stimulation. Cells were treated with 0.3–30 μM BIX02189 as an ERK5/MEK5 inhibitor (Selleck, Houston, TX, USA) or 0.1–10 μM DL-thiorphan as a neprilysin inhibitor (Enzo Life Sciences, Farmingdale, NY, USA) 1 h before G-CSF stimulation. After 24-h stimulation of $oA\beta_{1-42}$, neurons were fixed with 4% paraformaldehyde for 10 min and permeabilized with 0.1% Triton X-100 for 5 min at room temperature. After blocking with 5% goat serum for 1 h at room temperature, cells were stained with rabbit polyclonal anti-microtubule–associated protein (MAP)-2 antibody (1:1000, Millipore, Billerica, MA, USA), and Aβ was stained with mouse monoclonal anti-Aβ antibody (clone 4G8, 1:1000, Millipore). Images were analyzed with a deconvolution fluorescent microscope system (BZ-8000; Keyence, Osaka, Japan).

Assessments of neuronal survival

Neuronal survival was assessed by the number of MAP-2–positive neurons and 2-(2-methoxy-4-nitrophenyl)-3-(4-nitrophenyl)-5-(2,4-disulfophenyl)-2H-tetrazolium (WST-8) assay as previously described [15]. To count MAP-2–positive neurons and normalized based on results observed with untreated neurons. Viable neurons stained strongly with an anti–MAP-2 antibody, whereas damaged neurons showed much weaker staining. The number of MAP-2–positive neurons was counted in 10 random fields per well. More than 200 cells were examined in three independent trials. The number of untreated viable neurons was normalized to 100%.

Immunohistochemistry

Ten-micrometer-thick frozen sections of APP/PS1 Tg mouse brains were prepared using a previously described method [11]. Sections were permeabilized with 1% Triton X-100 after blocking with 10% normal goat serum for 30 min, and then were incubated with anti-Aβ mouse monoclonal antibody (clone 4G8, 1:500, Chemicon) overnight at 4°C. After rinsing, they were incubated with Alexa488-conjugated secondary antibody (1:1,000, Invitrogen) and 1 μg/ml Hoechst33342 for 1 h at room temperature. After rinsing, they were mounted in Fluoromount-G (SouthernBiotech). Images were analyzed with a deconvolution fluorescence microscope system (Keyence).

RNA extraction and reverse transcription-PCR (RT-PCR)

The mRNA expression of neprilysin was detected by RT-PCR. Neurons were plated at a density of 5×10^4 cells per well in 24-well multidishes, and stimulated with or without 100 ng/ml G-CSF (R&D Systems, Minneapolis, MN, USA) for 6 h. Total RNA was extracted from neurons using RNeasy Mini Kit (Qiagen, Valencia, CA, USA). cDNA synthesis was performed using SuperScript II (Invitrogen). PCR was carried out using the following primers.

neprilysin sense: 5′-GACCTTACTTGGATGGATGC-3′
neprilysin antisense: 5′-ACCATACACTGGGATTGGTC-3′
GAPDH sense: 5′-ACTCACGGCAAATTCAACG-3′
GAPDH antisense: 5′-CCCTGTTGCTGTAGCCGTA-3′

Measurement of protein level and enzymatic activity of NEP

The cell membrane fractions from the mouse primary neurons or the APP/PS1 Tg mouse brains were harvested and assessed for NEP protein levels using specific ELISA (R&D Systems). NEP enzymatic activity was also examined as described previously [16]. The fluorescence of each samples were measured by a Wallac 1420 $ARVO_{MX}$ (PerkinElmer Japan, Yokohama, Japan).

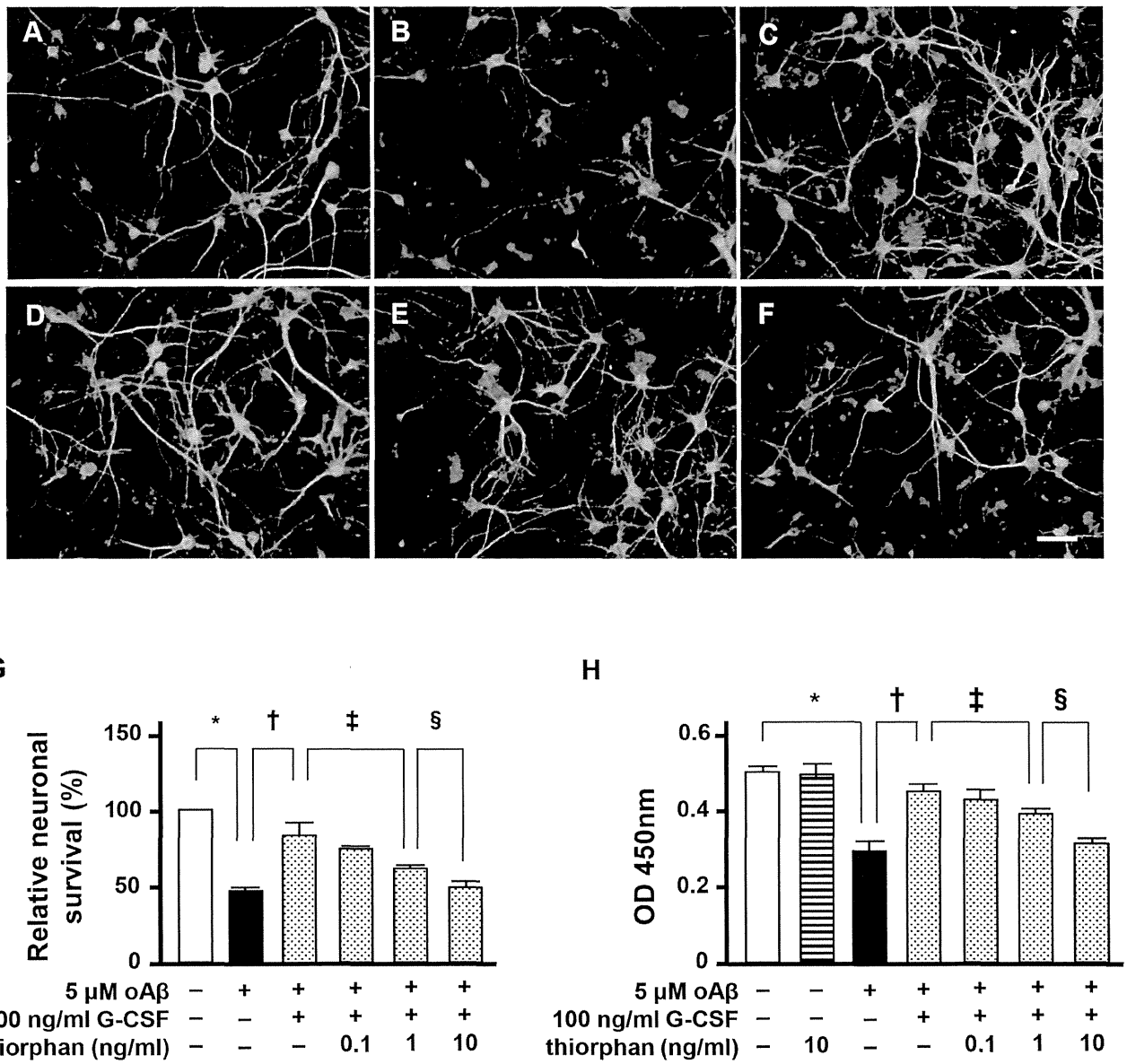

Figure 3. Neuroprotective effect of G-CSF depends on NEP. A–F, Fluorescent microscopic images of mouse primary cortical neuron cultures. A, Untreated neurons. B, Neurons treated with 5 μM $oA\beta_{1-42}$. C, Neurons treated with 5 μM $oA\beta_{1-42}$ and 100 ng/ml G-CSF. D, Neurons treated with 5 μM $oA\beta_{1-42}$, 100 ng/ml G-CSF and 0.1 ng/ml thiorphan. E, Neurons treated with 5 μM $oA\beta_{1-42}$, 100 ng/ml G-CSF and 1 ng/ml thiorphan. F, Neurons treated with 5 μM $oA\beta_{1-42}$, 100 ng/ml G-CSF and 10 ng/ml thiorphan. The NEP inhibitor canceled the neuroprotective effects of G-CSF. Neurons were stained with anti-MAP-2 antibodies (green) and Aβ was stained with 4G8 antibodies (red). Scale bar: 50 μm. G, Relative neuronal survival. The number of viable neurons (MAP-2–positive neurons) was quantified relative to results observed with untreated neurons. The NEP inhibitor dose-dependently suppressed the neuroprotective effects of G-CSF. *, $p<0.001$; †, $p<0.001$; ‡, $p<0.05$; §, $p<0.01$. Values are means ± SEM (n = 3). H, WST-8 assay. The NEP inhibitor reversed the neuroprotective effects of G-CSF in a dose-dependent manner. *, $p<0.001$; †, $p<0.001$; ‡, $p<0.05$; §, $p<0.01$. Values are means ± SEM (n = 6).
doi:10.1371/journal.pone.0103458.g003

Human Aβ ELISA

To evaluate $oA\beta_{1-42}$ in neuronal culture, we used a human Aβ oligomer specific ELISA kit (IBL, Gunma, Japan). Neurons were pre-treated with 10 μM thiorphan for 1 h and then treated with G-CSF for 3 h prior to the addition of 5 μM $oA\beta_{1-42}$ for 24 h. The neuronal culture supernatants were assessed with an ELISA kit. To evaluate the amount of human $A\beta_{1-40}$ and $A\beta_{1-42}$ in mouse brains, we used a human $A\beta_{1-40}$ and $A\beta_{1-42}$ specific ELISA kit (Wako Pure Chemical Industries, Osaka, Japan) as previously described [17]. Brains were homogenized with TNE lysis buffer [50 mM Tris-HCl at pH 7.6, 1% Nonidet P-40, 150 mM NaCl, 2 mM EDTA, and protease inhibitor mixture (Complete Mini EDTA-free, Roche, Germany)] and centrifuged at 10,000 *g* for 15 min at 4°C. The supernatants were analyzed by each Aβ specific ELISA kit. The values obtained were corrected with the wet weight of each brain sample.

Statistical Analysis

Statistical significance was analyzed with a Student's *t*-test or one-way analysis of variance followed by Tukey's post-hoc test

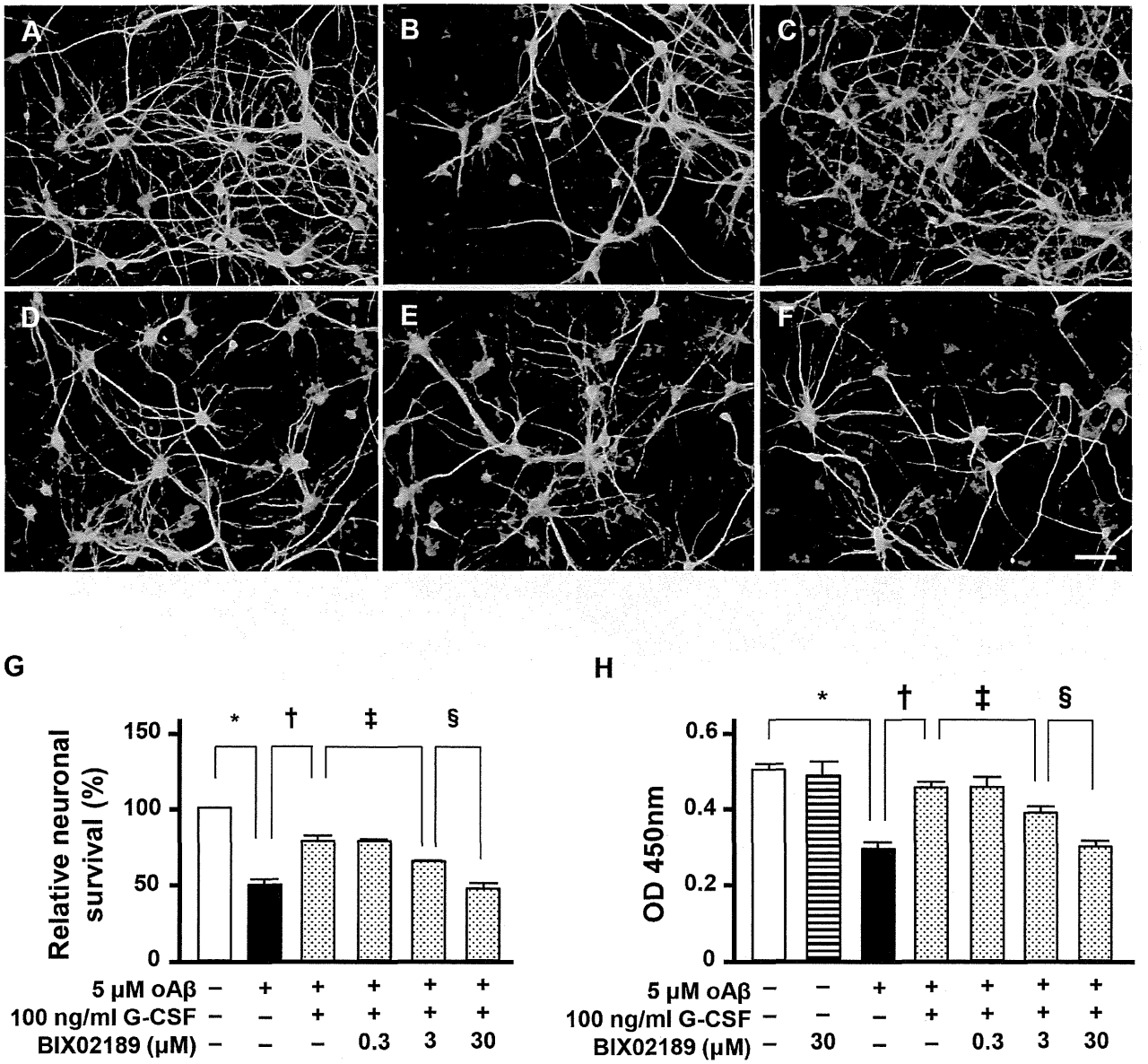

Figure 4. Neuroprotective effect of G-CSF requires MEK5/ERK5 signaling. A–F, Fluorescent microscopic images of mouse primary cortical neuron cultures. A, Untreated neurons. B, Neurons treated with 5 μM $oA\beta_{1-42}$. C, Neurons treated with 5 μM $oA\beta_{1-42}$ and 100 ng/ml G-CSF. D, Neurons treated with 5 μM $oA\beta_{1-42}$, 100 ng/ml G-CSF and 0.3 μM BIX02189. E, Neurons treated with 5 μM $oA\beta_{1-42}$, 100 ng/ml G-CSF and 3 μM BIX02189. F, Neurons treated with 5 μM $oA\beta_{1-42}$, 100 ng/ml G-CSF and 30 μM BIX02189. The MEK5/ERK5 inhibitor BIX02189 almost completely suppressed G-CSF–mediated protection against oAβ-induced neurotoxicity. Neurons were stained with anti–MAP-2 antibodies (green), and Aβ was stained with 4G8 antibodies (red). Scale bar: 50 μm. G, Relative neuronal survival. The number of viable neurons (MAP-2–positive neurons) was quantified relative to results observed with untreated neurons. Inhibition of MEK5/ERK5 almost completely ablated the neuroprotective effects of G-CSF. *, $p<0.001$; †, $p<0.001$; ‡, $p<0.001$. Values are means ± SEM (n = 3). H, WST-8 assay. Blocking MEK5/ERK5 almost completely canceled the neuroprotective effects of G-CSF. *, $p<0.001$; †, $p<0.001$; ‡, $p<0.001$. Values are means ± SEM (n = 6).
doi:10.1371/journal.pone.0103458.g004

using GraphPad Prism version 5.0 (GraphPad Software, La Jolla, CA, USA).

Results

G-CSF rescues $oA\beta_{1-42}$-induced neuronal damage

We first examined the effects of G-CSF on $oA\beta_{1-42}$-induced neurotoxicity using mouse primary neuronal culture (Figure 1). We found that treatment with 5 μM $oA\beta_{1-42}$ for 24 h resulted in severe neurotoxicity (Figure 1B; Figure 1F and 1G, black columns). Three hours before the addition of 5 μM $oA\beta_{1-42}$, we then applied 1–100 ng/ml G-CSF for 24 h. Treatment with G-CSF significantly suppressed $oA\beta_{1-42}$-induced neuronal damage in a dose-dependent manner (Figure 1C–E; Figure 1F and 1G, shaded columns).

G-CSF enhances oAβ degradation through activation of NEP

Next, we assessed whether G-CSF treatment alters the amount of Aβ applied in neuronal culture. We found that G-CSF

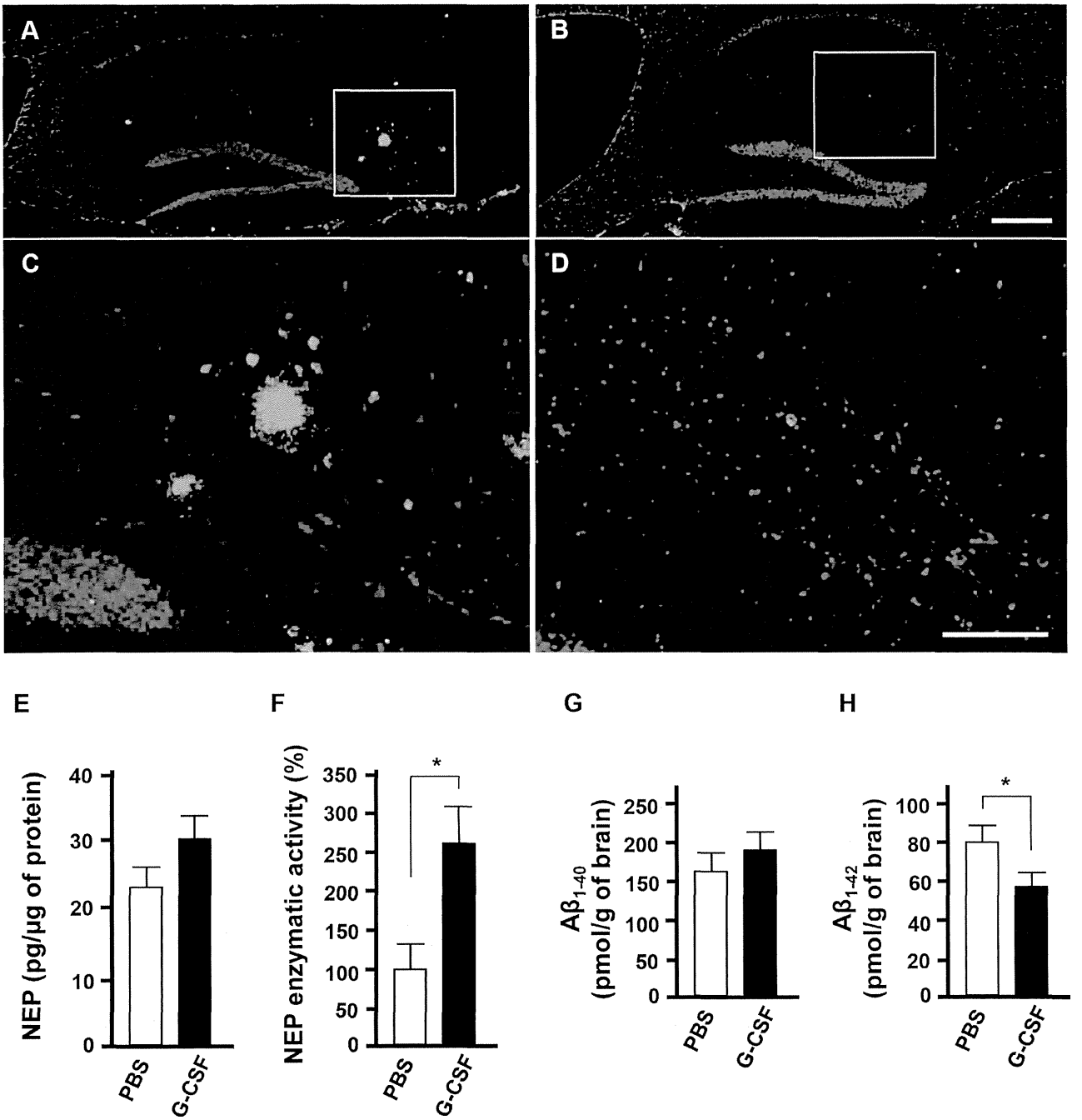

Figure 5. ***In vivo*** **G-CSF treatment enhances $A\beta_{1-42}$ degradation by activation of NEP.** A–D, Fluorescent microscopic images of hippocampi from 12-month-old APP/PS1 Tg mice. A, PBS-injected APP/PS1 Tg mice. B, G-CSF–injected APP/PS1 Tg mice. C, Higher magnification image of the white-framed area in A. D, Higher magnification image of the white-framed area in B. Green, Aβ (4G8); blue, nucleus (Hoechst). Scale bar; 200 μm in A and B, 100 μm in C and D. E, ELISA data for NEP. Values are means ± SEM (n = 3). F, NEP enzymatic activity assay. G-CSF treatment enhanced NEP enzymatic activity in APP/PS1 Tg mouse brains, whereas NEP protein levels were not affected. *, $p<0.05$. Values are means ± SEM (n = 3). G, ELISA data for human $A\beta_{1-40}$ in APP/PS1 Tg mouse brains. H, ELISA data for human $A\beta_{1-42}$ in APP/PS1 Tg mouse brains. G-CSF treatment significantly reduced $A\beta_{1-42}$ load, but not $A\beta_{1-40}$, in APP/PS1 Tg mice. *, $p<0.05$. Values are means ± SEM (n = 3).
doi:10.1371/journal.pone.0103458.g005

significantly decreased Aβ concentration in neuronal culture (Figure 2D, black column). We then assessed the expression levels of Aβ-degrading enzymes [NEP and insulin-degrading enzyme (IDE)] in G-CSF–treated neurons. RT-PCR data indicated that the addition of G-CSF upregulated the expression level of NEP in neurons, whereas IDE was not affected (Figure 2A and data not shown). Next, we assessed the protein levels and enzymatic activity of NEP. G-CSF treatment significantly enhanced NEP enzymatic activity, but not NEP protein level (Figure 2B and 2C). Inhibition of NEP by thiorphan completely reversed the amount of Aβ

(Figure 2D, dotted column), suggesting that Aβ degradation by G-CSF stems from the activation of neuronal NEP. Treatment with thiorphan alone did not affect the amount of Aβ.

NEP is critical for the neuroprotective effect of G-CSF

We assessed whether the neuroprotective effect of G-CSF results from NEP (Figure 3). We found that treatment with the NEP inhibitor thiorphan almost completely ablated the neuroprotective effects of G-CSF (Figure 3D–F; Figure 3G and 3H, shaded columns). These findings imply that treatment with G-CSF enhanced neuronal NEP activity and protected against oAβ_{1-42}-induced neurotoxicity through Aβ degradation.

The MEK5/ERK5 pathway contributes to G-CSF–mediated neuroprotection

The MEK5/ERK5 pathway is a major downstream effector of G-CSF signaling. We examined the role of the MEK5/ERK5 pathway in G-CSF–mediated neuroprotection. We found that inhibition of MEK5/ERK5 by BIX02189 almost completely suppressed the neuroprotective effects of G-CSF against oAβ-induced neurotoxicity (Figure 4D–F; Figure 4G and 4H, shaded columns). We confirmed BIX02189 decreased NEP activity in G-CSF-treated neurons. These results suggest that G-CSF–mediated neuroprotection depended on MEK5/ERK5 signaling.

In vivo G-CSF treatment enhances Aβ_{1-42} degradation by activation of NEP

Finally, we examined whether G-CSF treatment enhances NEP activity and Aβ degradation using APP/PS1 Tg mice, a mouse model of Alzheimer's disease. G-CSF was injected into the cerebral ventricular space of APP/PS1 mice. Three days after injection, mouse brains were assessed by histological and biochemical analysis. Histological analysis revealed that G-CSF treatment reduced the Aβ burden in the hippocampus, whereas PBS-treated mice showed substantial amounts of Aβ deposits (Figure 5A–D). As expected, G-CSF treatment significantly enhanced NEP activity in the brains of APP/PS1 Tg mice, whereas NEP protein levels were not affected (Figure 5E and 5F). Human Aβ-specific ELISAs also revealed that G-CSF injection significantly reduced the amount of Aβ_{1-42} in APP/PS1 transgenic mice, whereas Aβ_{1-40} load was not affected (Figure 5G and 5H).

Discussion

The present study revealed a novel neuroprotective function of G-CSF against oAβ toxicity. We found that G-CSF significantly enhanced neuronal NEP activity and led to increased degradation of oAβ. Furthermore, injection of G-CSF into the cerebral ventricular space of APP/PS1 mice also enhanced oAβ degradation by activation of NEP.

NEP is the major Aβ degrading peptidase. NEP deficiency results in elevated levels of endogenous Aβ_{1-40} and Aβ_{1-42} in the hippocampus, cortex, thalamus/striatum, and cerebellum [18]. NEP is also reported to degrade Aβ_{1-40} more rapidly than Aβ_{1-42} *in vitro* [19]. However, our in *vivo* data show that G-CSF reduced the amount of Aβ_{1-42} in APP/PS1 Tg mice, though Aβ_{1-40} was not affected. Clearance of Aβ_{1-40} may not depend on NEP-catalyzed proteolysis as that of Aβ_{1-42}. These results suggest that G-CSF has an effect on Aβ_{1-42} degradation via NEP activation *in vivo*. While NEP is capable of cleaving Aβ monomers, its ability to degrade oAβ is controversial [10]. However, a recent report shows that NEP gene transfer into an AD mouse model significantly reduces oAβ [20]. In the present study, we have shown that G-CSF treatment reduced the amount of oAβ in the supernatants of neuronal cultures via activation of NEP. Therefore, NEP is clearly able to degrade oAβ.

Another Aβ degrading enzyme, IDE, is reported to be reduced in the hippocampus of AD [21]. The enhanced IDE activity in IDE and APP double-transgenic mice decreases Aβ levels and prevents the formation of AD pathology. However, G-CSF did not induce activation of IDE in neurons in that study. The reduced level of oAβ was small. Other mechanism such as neurogenesis may be involved in neuroprotection.

G-CSF activates the Jak/Stat, MAPK (Erk1/2, JNK and p38), PI3-K, and Src family kinase cascades [22]. A recent study shows that the MEK5/ERK5 pathway is a major downstream effector of G-CSF signaling in the regulation of cell proliferation and survival. [23,24]. In the present study, inhibition of MEK5/ERK5 by BIX02189 almost completely suppressed the neuroprotective effects of G-CSF against oAβ-induced neurotoxicity. The results suggest that G-CSF–induced NEP is activated by the MEK5/ERK5 pathway. MEK5/ERK5 pathway is involved in cell proliferation, cell survival, and angiogenesis. However, the precise mechanism of NEP expression by MEK5/ERK5 remains unknown.

The G-CSF receptor is also expressed in microglia, and expression is increased after spinal cord injury [25]. G-CSF has been shown to promote the recruitment of microglia to the injury site, which regulates microglial activation by inhibiting the activity of NF-κB. [26]. In the previous study, G-CSF increased microglial burden, reduced Aβ deposition, and ameliorated the cognitive impairments in APP/PS1 mice. This mechanism is considered to be microglial Aβ clearance and neurogenesis in neural stem cells [9]. Therefore, microglial Aβ clearance may also contribute to decreasing the amount of Aβ_{1-42} by G-CSF injection in APP/PS1 transgenic mice in the present study. Taken together, the present study shows that G-CSF significantly enhances the expression level and enzymatic activity of NEP in neurons, indicating that G-CSF could be a useful therapeutic strategy against oAβ_{1-42} neurotoxicity in AD.

Author Contributions

Conceived and designed the experiments: YD HT TM AS. Performed the experiments: YD HT HM KF HH SJ JK BP YS TM. Analyzed the data: YD HT TM HH KF. Contributed reagents/materials/analysis tools: YD HT TM. Contributed to the writing of the manuscript: YD HT TM AS.

References

1. Busciglio J, Yankner BA (1995) Apoptosis and increased generation of reactive oxygen species in Down's syndrome neurons in vitro. Nature 378: 776–779.
2. Grace EA, Rabiner CA, Busciglio J (2002) Characterization of neuronal dystrophy induced by fibrillar amyloid beta: implications for Alzheimer's disease. Neuroscience 114: 265–273.
3. Walsh DM, Klyubin I, Fadeeva JV, Cullen WK, Anwyl R, et al. (2002) Naturally secreted oligomers of amyloid beta protein potently inhibit hippocampal long-term potentiation in vivo. Nature 416: 535–539.
4. Deshpande A, Mina E, Glabe C, Busciglio J (2006) Different conformations of amyloid beta induce neurotoxicity by distinct mechanisms in human cortical neurons. J Neurosci 26: 6011–6018.
5. Boneberg EM, Hareng L, Gantner F, Wendel A, Hartung T (2000) Human monocytes express functional receptors for granulocyte colony-stimulating factor that mediate suppression of monokines and interferon-gamma. Blood 95: 270–276.
6. Hartung T (1998) Anti-inflammatory effects of granulocyte colony-stimulating factor. Curr Opin Hematol 5: 221–225.

7. Schneider A, Kruger C, Steigleder T, Weber D, Pitzer C, et al. (2005) The hematopoietic factor G-CSF is a neuronal ligand that counteracts programmed cell death and drives neurogenesis. J Clin Invest 115: 2083–2098.
8. Tsai KJ, Tsai YC, Shen CK (2007) G-CSF rescues the memory impairment of animal models of Alzheimer's disease. J Exp Med 204: 1273–1280.
9. Sanchez-Ramos J, Song S, Sava V, Catlow B, Lin X, et al. (2009) Granulocyte colony stimulating factor decreases brain amyloid burden and reverses cognitive impairment in Alzheimer's mice. Neuroscience 163: 55–72.
10. Grimm MO, Mett J, Stahlmann CP, Haupenthal VJ, Zimmer VC, et al. (2013) Neprilysin and Abeta Clearance: Impact of the APP Intracellular Domain in NEP Regulation and Implications in Alzheimer's Disease. Front Aging Neurosci 5: 98.
11. Doi Y, Mizuno T, Maki Y, Jin S, Mizoguchi H, et al. (2009) Microglia activated with the toll-like receptor 9 ligand CpG attenuate oligomeric amyloid {beta} neurotoxicity in in vitro and in vivo models of Alzheimer's disease. Am J Pathol 175: 2121–2132.
12. Maurice T, Lockhart BP, Privat A (1996) Amnesia induced in mice by centrally administered beta-amyloid peptides involves cholinergic dysfunction. Brain Res 706: 181–193.
13. Alkam T, Nitta A, Mizoguchi H, Itoh A, Nabeshima T (2007) A natural scavenger of peroxynitrites, rosmarinic acid, protects against impairment of memory induced by Abeta(25–35). Behav Brain Res 180: 139–145.
14. Takeuchi H, Mizuno T, Zhang G, Wang J, Kawanokuchi J, et al. (2005) Neuritic beading induced by activated microglia is an early feature of neuronal dysfunction toward neuronal death by inhibition of mitochondrial respiration and axonal transport. J Biol Chem 280: 10444–10454.
15. Doi Y, Takeuchi H, Horiuchi H, Hanyu T, Kawanokuchi J, et al. (2013) Fingolimod phosphate attenuates oligomeric amyloid beta-induced neurotoxicity via increased brain-derived neurotrophic factor expression in neurons. PLoS One 8: e61988.
16. Hemming ML, Selkoe DJ, Farris W (2007) Effects of prolonged angiotensin-converting enzyme inhibitor treatment on amyloid beta-protein metabolism in mouse models of Alzheimer disease. Neurobiol Dis 26: 273–281.
17. Takeuchi H, Mizoguchi H, Doi Y, Jin S, Noda M, et al. (2011) Blockade of gap junction hemichannel suppresses disease progression in mouse models of amyotrophic lateral sclerosis and Alzheimer's disease. PLoS One 6: e21108.
18. Iwata N, Tsubuki S, Takaki Y, Shirotani K, Lu B, et al. (2001) Metabolic regulation of brain Abeta by neprilysin. Science 292: 1550–1552.
19. Shirotani K, Tsubuki S, Iwata N, Takaki Y, Harigaya W, et al. (2001) Neprilysin degrades both amyloid beta peptides 1–40 and 1–42 most rapidly and efficiently among thiorphan- and phosphoramidon-sensitive endopeptidases. J Biol Chem 276: 21895–21901.
20. Iwata N, Sekiguchi M, Hattori Y, Takahashi A, Asai M, et al. (2013) Global brain delivery of neprilysin gene by intravascular administration of AAV vector in mice. Sci Rep 3: 1472.
21. Zhao Z, Xiang Z, Haroutunian V, Buxbaum JD, Stetka B, et al. (2007) Insulin degrading enzyme activity selectively decreases in the hippocampal formation of cases at high risk to develop Alzheimer's disease. Neurobiol Aging 28: 824–830.
22. Leissring MA, Farris W, Chang AY, Walsh DM, Wu X, et al. (2003) Enhanced proteolysis of beta-amyloid in APP transgenic mice prevents plaque formation, secondary pathology, and premature death. Neuron 40: 1087–1093.
23. Avalos BR (1996) Molecular analysis of the granulocyte colony-stimulating factor receptor. Blood 88: 761–777.
24. Dong F, Gutkind JS, Larner AC (2001) Granulocyte colony-stimulating factor induces ERK5 activation, which is differentially regulated by protein-tyrosine kinases and protein kinase C. Regulation of cell proliferation and survival. J Biol Chem 276: 10811–10816.
25. Yamasaki R, Tanaka M, Fukunaga M, Tateishi T, Kikuchi H, et al. (2010) Restoration of microglial function by granulocyte-colony stimulating factor in ALS model mice. J Neuroimmunol 229: 51–62.
26. Guo Y, Zhang H, Yang J, Liu S, Bing L, et al. (2013) Granulocyte colony-stimulating factor improves alternative activation of microglia under microenvironment of spinal cord injury. Neuroscience 238: 1–10.

OPEN ACCESS Freely available online

PLOS | ONE

Evidence for Aberrant Astrocyte Hemichannel Activity in Juvenile Neuronal Ceroid Lipofuscinosis (JNCL)

Maria Burkovetskaya[1☯], Nikolay Karpuk[1☯], Juan Xiong[1], Megan Bosch[2], Michael D. Boska[3], Hideyuki Takeuchi[4], Akio Suzumura[4], Tammy Kielian[1*]

1 Departments of Pathology and Microbiology, University of Nebraska Medical Center, Omaha, Nebraska, United States of America, **2** Departments of Pharmacology and Experimental Neuroscience, University of Nebraska Medical Center, Omaha, Nebraska, United States of America, **3** Department of Radiology, University of Nebraska Medical Center, Omaha, Nebraska, United States of America, **4** Department of Neuroimmunology, Research Institute of Environmental Medicine, Nagoya University, Nagoya, Japan

Abstract

Juvenile Neuronal Ceroid Lipofuscinosis (JNCL) is a lysosomal storage disease caused by an autosomal recessive mutation in *CLN3* that leads to vision loss, progressive cognitive and motor decline, and premature death. Morphological evidence of astrocyte activation occurs early in the disease process and coincides with regions where neuronal loss eventually ensues. However, the consequences of CLN3 mutation on astrocyte function remain relatively ill-defined. Astrocytes play a critical role in CNS homeostasis, in part, by their ability to regulate the extracellular milieu via the formation of extensive syncytial networks coupled by gap junction (GJ) channels. In contrast, unopposed hemichannels (HCs) have been implicated in CNS pathology by allowing the non-discriminant passage of molecules between the intracellular and extracellular milieus. Here we examined acute brain slices from CLN3 mutant mice ($CLN3^{\Delta ex7/8}$) to determine whether CLN3 loss alters the balance of GJ and HC activity. $CLN3^{\Delta ex7/8}$ mice displayed transient increases in astrocyte HC opening at postnatal day 30 in numerous brain regions, compared to wild type (WT) animals; however, HC activity steadily decreased at postnatal days 60 and 90 in $CLN3^{\Delta ex7/8}$ astrocytes to reach levels lower than WT cells. This suggested a progressive decline in astrocyte function, which was supported by significant reductions in glutamine synthetase, GLAST, and connexin expression in $CLN3^{\Delta ex7/8}$ mice compared to WT animals. Based on the early increase in astrocyte HC activity, $CLN3^{\Delta ex7/8}$ mice were treated with the novel carbenoxolone derivative INI-0602 to inhibit HCs. Administration of INI-0602 for a one month period significantly reduced lysosomal ceroid inclusions in the brains of $CLN3^{\Delta ex7/8}$ mice compared to WT animals, which coincided with significant increases in astrocyte GJ communication and normalization of astrocyte resting membrane potential to WT levels. Collectively, these findings suggest that alterations in astrocyte communication may impact the progression of JNCL and could offer a potential therapeutic target.

Citation: Burkovetskaya M, Karpuk N, Xiong J, Bosch M, Boska MD, et al. (2014) Evidence for Aberrant Astrocyte Hemichannel Activity in Juvenile Neuronal Ceroid Lipofuscinosis (JNCL). PLoS ONE 9(4): e95023. doi:10.1371/journal.pone.0095023

Editor: Jun-ichi Kira, Kyushu University, Japan

Received December 19, 2013; **Accepted** March 23, 2014; **Published** April 15, 2014

Funding: This work was supported by the National Institutes of Health National Institute of Neurological Disorders and Stroke (R21NS084392), Batten Disease Support and Research Administration (BDSRA), Bee For Battens - The Saoirse Foundation, and the UNMC Dean's Pediatric Research Fund (to T.K.). J.X. is supported by a UNMC-Chinese Scholarship Council fellowship. The development of INI-0602 was supported by the Program for Promotion of Fundamental Studies in Health Sciences of the National Institute of Biomedical Innovation (NIBIO) of Japan (to H.T. and A.S.). The funders had no role in study design, data collection and analysis, decision to publish, or preparation of the manuscript.

Competing Interests: The authors have declared that no competing interests exist.

* E-mail: tkielian@unmc.edu

☯ These authors contributed equally to this work.

Introduction

Juvenile Neuronal Ceroid Lipofuscinosis (JNCL), or Juvenile Batten Disease, is an autosomal recessively inherited lysosomal storage disorder caused by mutations in the *CLN3* gene [1]. In general, children with JNCL develop neurological symptoms beginning at 5–8 years of age typified by vision loss, behavioral disturbances, and seizure activity. The disease is associated with progressive neurological decline, involving substantial motor and cognitive loss and premature death by the late-teens to early 20 s [2,3]. The CNS is particularly vulnerable in JNCL, although systemic complications are also observed, since inclusions form in multiple cell types in the body [4]. In the CNS, neuronal loss is more pronounced in specific thalamocortical structures, including the thalamic nuclei, neocortex, substantia nigra, hippocampus, and cerebellum [5,6,7,8]. CLN3 mutation leads to the progressive accumulation of autofluorescent ceroid inclusions in the lysosome, which are predominantly composed of mitochondrial ATP synthase subunit c [9,10]. Interestingly, similar inclusions can occur in the aged brain, commonly referred to as lipofuscin, which can be detected in Alzheimer's or Parkinson's disease patients [11,12,13,14]. This suggests the possibility of common underlying pathologies between these neurodegenerative disorders, and although JNCL presents within the first decade of life, it is notable that these children progress to develop Parkinson-like symptoms that coincide with neuronal loss in the substantia nigra [15]. Indeed, evidence is emerging suggesting conserved autophagy and mitochondrial abnormalities associated with NCLs and adult-onset neurodegenerative diseases [16,17]. This suggests that studies investigating mechanisms of CNS dysfunction during

JNCL may also unveil novel pathways common to other neurodegenerative disorders.

Astrocytes and microglia are key contributors to neuronal homeostasis and function [18,19]. Prior studies using CLN3 knockout mice or animals where exons 7 and 8 of the *CLN3* gene were disrupted ($CLN3^{\Delta ex7/8}$), demonstrated early signs of glial activation that preceded neuronal loss [8,20]. Specifically, morphological evidence of glial activation was apparent by postnatal day 7; however, neuronal death was significantly delayed in comparison (i.e. apparent around 6–8 months). These findings suggest that chronic glial activation may provide extrinsic signals that influence neuronal survival at later disease intervals, although intrinsic defects in neurons cannot be ignored. Indeed, we recently reported that primary microglia from $CLN3^{\Delta ex7/8}$ mice are primed towards a proinflammatory phenotype and secrete heightened levels of numerous inflammatory mediators following exposure to stimuli that are elevated in the JNCL brain [21]. In addition, $CLN3^{\Delta ex7/8}$ microglia displayed constitutive caspase-1 activity, which when inhibited resulted in enhanced glutamate release via hemichannel action that induced $CLN3^{\Delta ex7/8}$ neuron death [21]. In contrast, limited information is currently available concerning the functional implications of CLN3 mutation in astrocytes. Since astrocytes play a central role in maintaining CNS homeostasis [22,23], glucose availability [24], and neurotransmitter utilization, pathological alterations in astrocyte activity in the context of CLN3 mutation may contribute to neuronal death during JNCL. If correct, identifying ways to reverse astrocyte dysfunction to reinstate normal attributes may promote neuronal survival.

Hemichannels (HCs) are non-selective pores located predominantly in the plasma membrane, which permit the free passage of various ions and small organic molecules (<1.5 kDa) between the extracellular and intracellular milieus. Although still an area of debate, numerous reports have revealed that astrocyte HCs are composed of connexin 43 (Cx43), whereas others have described pannexin involvement [25,26]. Two Cx HCs from neighboring astrocytes can interact to form a gap junction (GJ) channel. Numerous GJ channels organize astrocytes into broad syncytial networks, facilitating the rapid exchange of intracellular contents in a process referred to as GJ communication (GJC) [27,28,29,30,31]. Astrocyte GJC plays a role in the homeostatic regulation of extracellular pH, K^+, and glutamate levels [32,33,34]. Astrocytes also influence CNS vascular tone and neuronal synapses, which are facilitated, in part, via GJC [35,36,37,38]. Therefore, the balance between astrocyte GJC versus HC activity in the context of CLN3 mutation could influence the homeostatic balance of the CNS milieu and impact neuronal viability. Here we investigated the status of astrocyte GJC/HC activity and associated intrinsic electrophysiological properties using acute brain slices from $CLN3^{\Delta ex7/8}$ mice at three postnatal stages that significantly precede neuronal loss [8,20]. Postnatal day 30 was selected as a starting point for our experiments, since this generally extrapolates to an age when a positive diagnosis of JNCL is made in children [39,40], with the eventual goal of identifying abnormalities that could be targeted to delay/prevent neuronal loss during later stages of JNCL. This study is the first to report astrocyte communication and electrophysiological defects in the context of JNCL and importantly, our use of living brain slices provides an excellent model to assess the interplay between astrocytes and other CNS cell types.

Previous work by us and others has demonstrated that astrocyte HC activity is enhanced during neuroinflammatory conditions [41,42,43]. Since other forms of Batten Disease have been associated with neuroinflammation, the severity of which depends on the specific disease type [44,45,46,47], we were interested in examining whether astrocyte HC activity was modulated in JNCL. Here we report that $CLN3^{\Delta ex7/8}$ astrocytes in acute brain slices displayed increased HC activity in the majority of brain regions examined at postnatal day 30, which coincided with altered electrophysiological properties. However, these changes were transient, in that $CLN3^{\Delta ex7/8}$ astrocyte HC activity gradually decreased between postnatal days 60 and 90, and in some instances was lower than astrocytes from WT brain slices, suggesting a progressive deterioration in $CLN3^{\Delta ex7/8}$ astrocyte activity. Evidence to support a decline in astrocyte function was demonstrated by the fact that several molecules associated with glutamate homeostasis (i.e. glutamine synthetase and the glutamate-aspartate transporter GLAST) were significantly decreased in $CLN3^{\Delta ex7/8}$ mice at postnatal day 90. In contrast, GFAP expression was significantly elevated in several brain regions of $CLN3^{\Delta ex7/8}$ animals, in agreement with previous reports [8,20], indicating that the decreases in GLAST and glutamine synthetase detected in $CLN3^{\Delta ex7/8}$ mice is not the result of astrocyte loss. Rather, these findings reveal the attrition of molecules that regulate glutamate homeostasis, which likely triggers astrocyte activation in an attempt to rectify this decline. Treatment of $CLN3^{\Delta ex7/8}$ mice with the carbenoxolone (CBX) derivative INI-0602 to block elevated HC activity at postnatal day 30, led to improvements in several pathological changes typical of JNCL, including significant reductions in lysosomal ceroid inclusions within the CNS, which coincided with enhanced GJC. Collectively, these results suggest that astrocyte dysfunction is evident during early JNCL and that modulation of GJC/HC activity may represent a promising target to reverse some pathological outcomes typical of the disease.

Results

Use of CellTracker Blue (CTB) to Visualize Live Astrocytes in Acute Brain Slices

Before we initiated our analysis of HC activity in $CLN3^{\Delta ex7/8}$ astrocytes, a method was needed to reliably identify cells in acute brain slices. Since the fluorescent dyes ethidium bromide (EtBr) and sulforhodamine 101 (SR101), which are commonly used for assessing HC activity and astrocyte identification, respectively [41,48], have overlapping wavelengths, we examined a panel of fluorescent molecules that could be used for astrocyte detection with excitation/emission properties distinct from EtBr. This led us to develop a staining protocol using the fluorescent dye CTB (7-amino-4-chloromethylcoumarin, CMAC). CTB is a membrane-permeable thiol-reactive probe, which undergoes a glutathione *S*-transferase–mediated reaction intracellularly to produce a membrane-impermeable glutathione fluorescent adduct [49,50]. Importantly, astrocytes are rich in glutathione [51] and can be clearly distinguished from neurons by CTB staining in most brain regions based on their size and morphological characteristics [49,50]. To confirm astrocyte staining with CTB in acute brain slices, we utilized GFAP-GFP transgenic mice, where both CTB and the classical astrocyte-selective dye SR101 were found to overlap with $GFAP\text{-}GFP^+$ astrocytes (Figure 1A). To further confirm CTB uptake in astrocytes, we performed immunofluorescence staining for the astrocyte-specific molecules GFAP and glutamine synthetase. CTB showed extensive overlap with both GFAP and glutamine synthetase in numerous brain regions, including the HPC and S1C (Figure 1B, and data not shown). Importantly, MAP2 and Iba-1 staining, to assess CTB uptake in neurons and microglia, respectively, revealed no co-localization with CTB in either population (Figure 1B), confirming that astrocytes are the

primary cell type labeled by CTB in acute brain slices. Moreover, patch-clamp recordings of live CTB^+ cells in acute brain slices confirmed that cells possessed characteristic astrocyte properties in several brain regions (data not shown). Based on this evidence, we conclude that the vast majority of CTB stained cells in live brain slices were astrocytes. Although it remains possible that other CNS cell types may internalize CTB, especially when higher dye concentrations are utilized, this was not a concern in our studies, since CTB levels were low (i.e. 2 μM). Because CTB displayed consistent cellular retention properties and photostability, and fluorescent emission was not promiscuous across other wavelengths, CTB was utilized in these studies to identify astrocytes when measuring HC activity in acute brain slices from $CLN3^{\Delta ex7/8}$ and WT mice.

Region- and Age-dependent Accumulation of Lysosomal Ceroid Inclusions in $CLN3^{\Delta ex7/8}$ Mice

The $CLN3^{\Delta ex7/8}$ mouse model of JNCL displays increased accumulation of autofluorescent ceroid inclusions, which is evident at early postnatal ages [52]. To facilitate downstream comparisons in astrocyte HC/GJ activity with disease pathology, we first evaluated the extent of ceroid inclusions in $CLN3^{\Delta ex7/8}$ mice, focusing on brain regions where subsequent analysis of astrocyte HC activity was performed. In agreement with previous reports [52], neurons displayed the most prominent accumulation of inclusions, although smaller deposits of storage material were also observed in CTB stained astrocytes (Figure 2A). In general, inclusion formation progressively increased with age in $CLN3^{\Delta ex7/8}$ mice in all five brain regions examined (Figure 2B). Intracellular accumulation of lipofuscin is a natural process associated with aging and, as such, WT animals also displayed a low degree of inclusion material [14]. However, inclusions were significantly higher in $CLN3^{\Delta ex7/8}$ animals in the S1C, VC, and TH at all ages compared to WT mice (Figure 2B). Interestingly, the HPC had low inclusion burdens at all three time points examined, even for $CLN3^{\Delta ex7/8}$ animals. This may be explained by the fact that the stratum radiatum layer of the hippocampus, which was examined here, has few neurons. Notably, the most pronounced expansion of inclusions in $CLN3^{\Delta ex7/8}$ mice occurred between postnatal days 30 and 60 in all five brain regions examined, whereas increases were less pronounced between days 60 and 90 (Figure 2B). Based on this analysis, the severity of inclusion deposition in $CLN3^{\Delta ex7/8}$ mice was ranked from most to least affected, namely TH<S1C< VC<STR<HPC. This relationship may be influenced by the relative numbers of neuronal cell bodies present in each structure, since neurons readily accumulate storage material. No significant differences in ceroid deposition were observed between male and female $CLN3^{\Delta ex7/8}$ animals (data not shown).

$CLN3^{\Delta ex7/8}$ Astrocytes Display Transient Region-dependent Increases in HC Activity that Decline with Advancing Age

Astrocytes are recognized for their role in maintaining tissue homeostasis, energy metabolism, and cell-cell communication, in part, through GJ and HC function [25,26]. Both astrocyte HC and GJ activity can be dramatically affected during pathological conditions and in some neurological diseases [41,42,43], which likely perturbs CNS homeostasis and the brain metabolome.

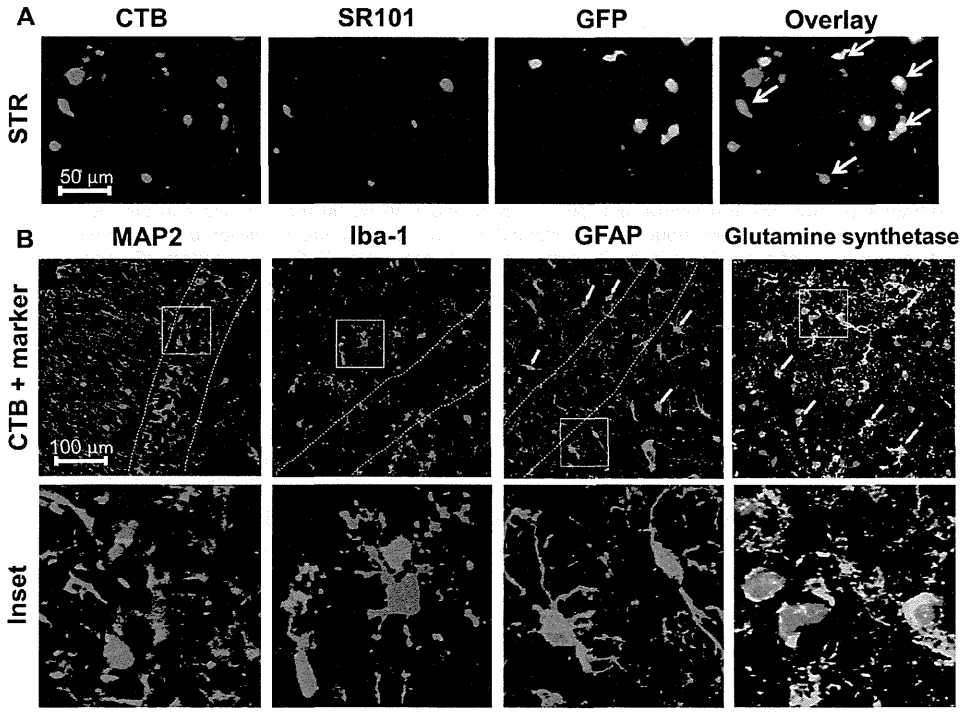

Figure 1. CellTracker Blue (CTB) co-localizes with traditional astrocyte markers. (A) Striatal (STR) brain slices from GFAP-GFP mice were stained with the astrocyte-selective dye sulforhodamine 101 (SR101) and CellTracker Blue (CTB). GFAP-GFP^+ astrocytes (green) and $SR101^+$ astrocytes (red) demonstrated a high degree of overlap with CTB (depicted by arrows in the overlay image). (B) CTB stained brain slices from the hippocampus (HPC) or S1C were fixed and sectioned, whereupon immunofluorescence staining was performed for the astrocyte-specific markers GFAP and glutamine synthetase as well as MAP2 and Iba-1 to identify neurons and microglia, respectively. The pyramidal layer of the HPC is delineated with dashed lines. Astrocytes demonstrating overlap with CTB and GFAP or glutamine synthetase are indicated by arrows.
doi:10.1371/journal.pone.0095023.g001

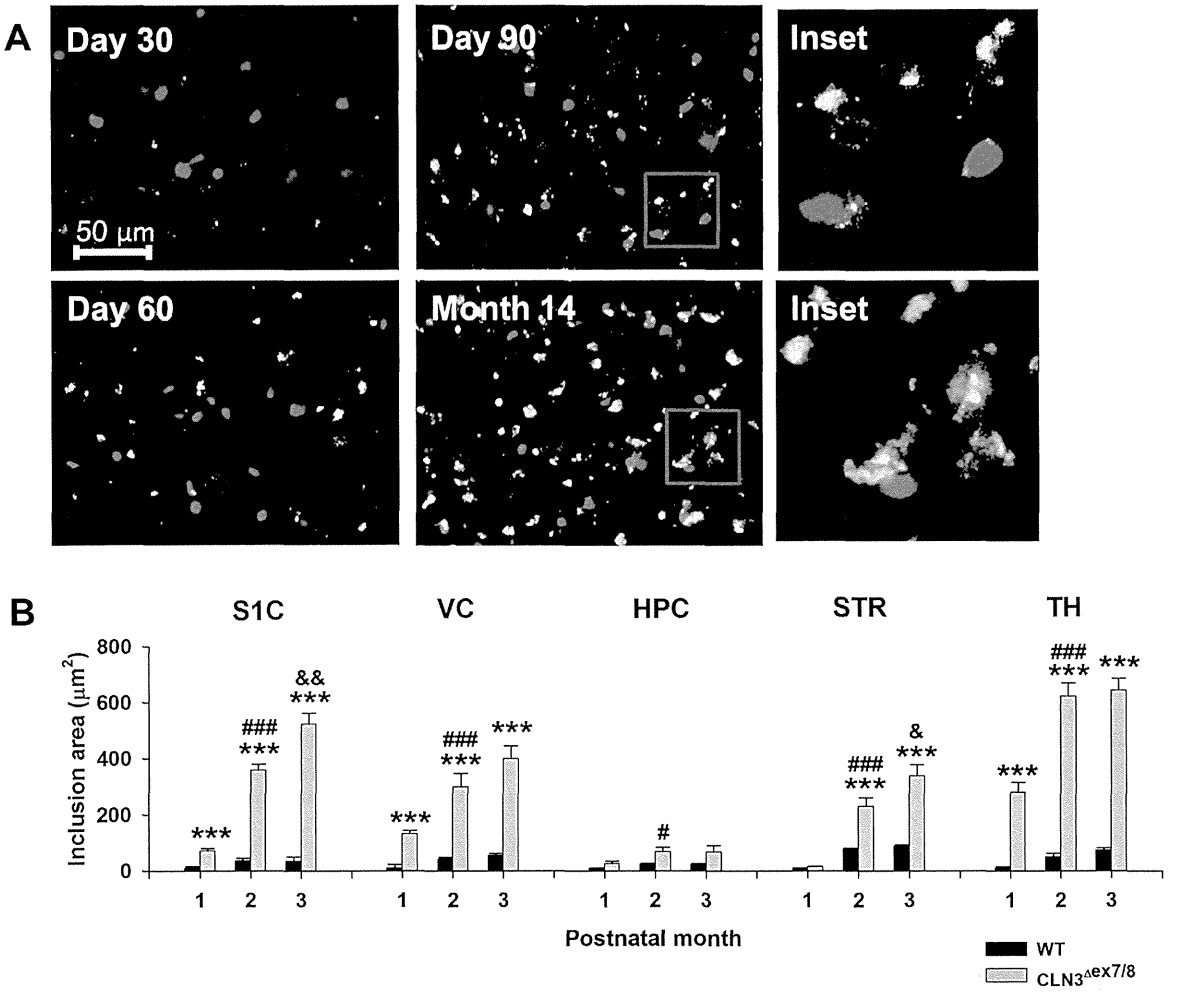

Figure 2. CLN3$^{\Delta ex7/8}$ mice display age- and region-dependent accumulation of lysosomal ceroid inclusions. (A) Examples of autofluorescent ceroid inclusions in acute brain slices from the visual cortex of CLN3$^{\Delta ex7/8}$ mice at day 30, 60, 90 and 14 months. Inclusions are visible in both the GFP (green) and rhodamine (red) filters (overlay = yellow-orange). CTB stained astrocyte soma (blue) displayed only a few intracellular inclusions (see insets). (B) Age-dependent accumulation of ceroid inclusions within the somatosensory cortex (S1C), visual cortex (VC), hippocampus (HPC), striatum (STR), and thalamus (TH) of wild type (WT) and CLN3$^{\Delta ex7/8}$ mice (5–8 animals per group). Significant differences between WT and CLN3$^{\Delta ex7/8}$ tissues are denoted by asterisks (***$p<0.001$), whereas changes between CLN3$^{\Delta ex7/8}$ tissues at postnatal days 30 and 60 within the same brain region are indicated by hatched signs (#, $p<0.05$; ###, $p<0.001$), and differences between CLN3$^{\Delta ex7/8}$ tissues at postnatal days 60 and 90 are indicated by ampersands (&&, $p<0.01$).
doi:10.1371/journal.pone.0095023.g002

Therefore, we examined HC and GJ activity of CLN3$^{\Delta ex7/8}$ and WT astrocytes in the same five brain regions with advancing age, to determine whether a link could be established between changes in astrocyte communication and ceroid accumulation. We elected to study younger animals with the eventual goal of identifying abnormalities that could be targeted to delay/prevent neuronal loss during later stages of JNCL. HC activity was significantly increased in CLN3$^{\Delta ex7/8}$ astrocytes at postnatal day 30 in four of the five brain regions examined, including the S1C, VC, STR, and TH (Figure 3A). However, increased HC opening in CLN3$^{\Delta ex7/8}$ mice was transient, where, in general, HC activity progressively decreased compared to WT animals at postnatal days 60 and 90 (Figure 3A). Interestingly, although HC activity steadily declined in CLN3$^{\Delta ex7/8}$ mice, it remained relatively stable in WT animals across postnatal days 30–90 (Figure 3B). The S1C of CLN3$^{\Delta ex7/8}$ mice were unique in that this region maintained open astrocyte HCs at postnatal day 60, whereas other brain areas displayed decreased activity. No differences in astrocyte HC activity were detected between male and female CLN3$^{\Delta ex7/8}$ mice (data not shown).

We next examined astrocyte GJC in the S1C and HPC during whole-cell patch clamp recordings. Only two brain regions could be examined due to the time-intensive nature of electrophysiology studies. No significant differences were observed between CLN3$^{\Delta ex7/8}$ and WT astrocytes in the S1C at any postnatal day examined (Figure S1). In contrast, GJC was significantly increased in CLN3$^{\Delta ex7/8}$ astrocytes in the HPC at postnatal day 90 compared to WT cells (40.2 ± 2.6, $n=18$ vs. 31.3 ± 2.7, $n=15$, respectively; $p<0.05$) (Figure S1). Collectively, these results are the first to demonstrate changes in astrocyte HC/GJ activity in the context of CLN3 mutation, which may have an impact on disease progression.

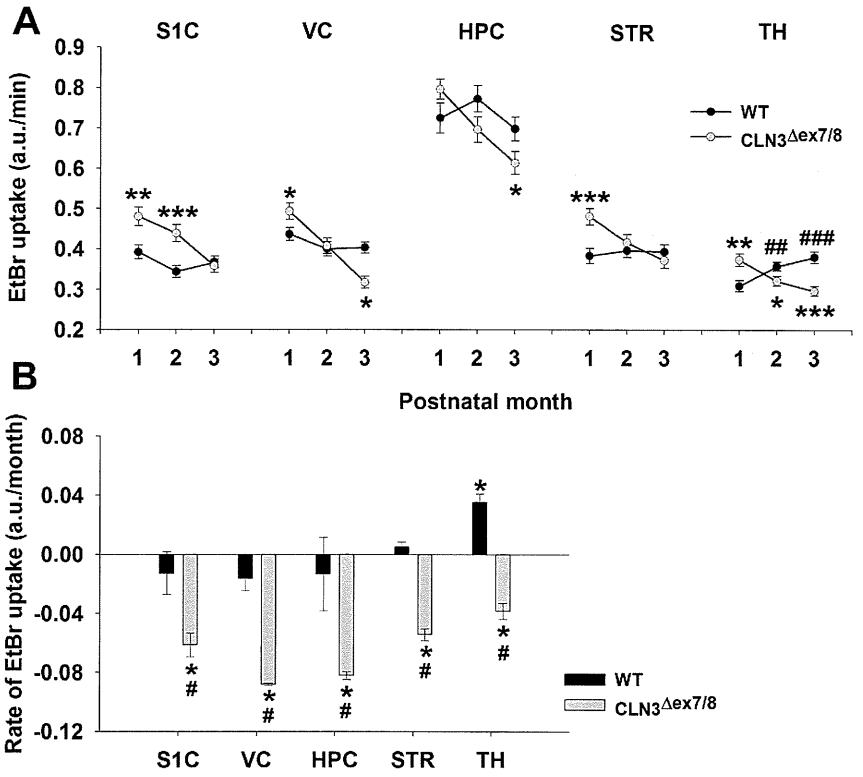

Figure 3. CLN3$^{\Delta ex7/8}$ astrocytes display transient region-dependent increases in hemichannel (HC) activity that decline with advancing age. Acute brain slices were prepared from wild type (WT) and CLN3$^{\Delta ex7/8}$ mice at postnatal days 30, 60 and 90, whereupon (A) EtBr uptake was measured in astrocytes in the somatosensory cortex (S1C), visual cortex (VC), hippocampus (HPC), striatum (STR), and thalamus (TH) as a quantitative measure of HC activity, which is expressed in arbitrary units (a.u.) per min. (B) Linear regression coefficients were determined for each brain region over time using the data shown in (A) and are presented as a.u. per month. Significant differences between WT and CLN3$^{\Delta ex7/8}$ astrocyte HC activity are indicated by asterisks (*$p<0.05$; **$p<0.01$; ***$p<0.001$), whereas changes within either WT or CLN3$^{\Delta ex7/8}$ astrocytes in the same brain region over time are denoted by hatched signs (#, $p<0.05$; ##, $p<0.01$; ###, $p<0.001$).
doi:10.1371/journal.pone.0095023.g003

CLN3 Mutation is Associated with the Decreased Expression of Molecules Involved in Glutamate Homeostasis

We next investigated whether the observed changes in CLN3$^{\Delta ex7/8}$ astrocyte HC activity coincided with alterations in the expression of key proteins implicated in CNS homeostasis. In particular, molecules important for glutamate regulation were examined given the reported role of glutamate excitotoxicity during JNCL [53,54,55]. We chose to utilize immunofluorescence staining and confocal microscopy to obtain maximal image resolution; however, we first needed to address the autofluorescent ceroid inclusions in CLN3$^{\Delta ex7/8}$ mice, which can interfere with the detection of target proteins by immunofluorescence staining and confound data interpretation. This issue was resolved by incubating tissue sections with Sudan black, which quenched the autofluorescence associated with CLN3$^{\Delta ex7/8}$ tissues (Figure S2). Sudan Black is known to interact with lipophilic inclusions several disorders, including Batten disease [56,57] and is widely used for attenuating undesirable autofluorescence in numerous tissues [58]. This approach allowed us to evaluate the expression of key astrocyte molecules in CLN3$^{\Delta ex7/8}$ mice using immunofluorescence staining methods.

Cx43 is a main component of astrocyte GJs and HCs, although Cx30 and pannexin 1 have also been implicated in GJ and HC formation, respectively [25,26]. We next quantitated Cx43 and Cx30 staining in the same five brain regions of CLN3$^{\Delta ex7/8}$ and WT mice where HC function was assessed, to determine whether protein expression coincided with the observed changes in astrocyte HC activity. Protein levels were only examined at postnatal day 90 since this was the latest interval assessed in this study and therefore, would represent the most severe pathology compared to earlier time points. Interestingly, Cx43 expression was significantly lower in the S1C, VC, STR, and TH of CLN3$^{\Delta ex7/8}$ mice compared to WT animals (Figure 4A and C) but not in the HPC, where GJC was significantly increased in CLN3$^{\Delta ex7/8}$ mice at the same age (i.e. postnatal day 90; Figure S1). In contrast, Cx30 was more variable, with expression significantly decreased and increased in the VC and TH, respectively, whereas other brain regions displayed similar levels (Figure 4A and B).

Glutamine synthetase plays an important role in glutamate metabolism, converting glutamate into glutamine, the latter of which is utilized as a substrate for glutamate production in neurons [19]. In addition, glutamate levels are elevated in the brains of JNCL patients and CLN3 mutant mice [59,60,61], and since astrocytes exclusively express glutamate synthetase in the CNS, altered enzyme levels could represent a key mechanism responsible for glutamate accumulation in the JNCL brain. Likewise, the glutamate transporter GLAST is a key pathway for glutamate uptake in astrocytes and could also be implicated in progressive disease pathology. Similar to Cx43, both glutamate synthetase and GLAST expression were significantly reduced in CLN3$^{\Delta ex7/8}$ mice

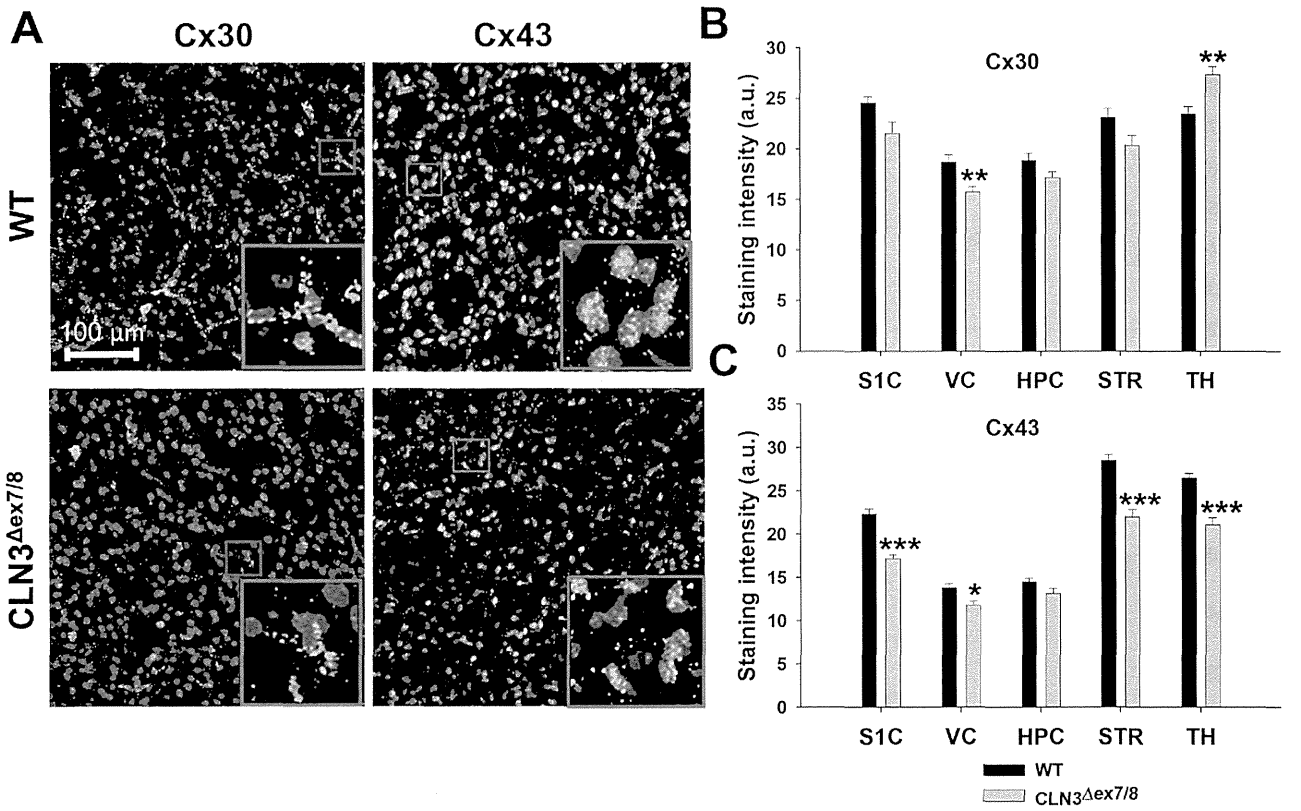

Figure 4. Connexin expression is significantly reduced in CLN3$^{\Delta ex7/8}$ astrocytes in a region-dependent manner. Immunofluorescence staining for Cx30 and Cx43 was performed on tissue sections from the somatosensory cortex (S1C), visual cortex (VC), hippocampus (HPC), striatum (STR), and thalamus (TH) of wild type (WT) and CLN3$^{\Delta ex7/8}$ mice at postnatal day 90. (A) Representative images depicting Cx30 and Cx43 expression in the STR with nuclei depicted by DAPI staining (blue; magnification, 20X; inset 50×50 μm zoom). (B) Cx30 and (C) Cx43 immunoreactivity was quantitated in each brain region (n = 3–4 mice per group; 6 images/region for each animal) with results reported in arbitrary units (a.u.). Significant differences in Cx30 and Cx43 staining between WT and CLN3$^{\Delta ex7/8}$ tissues are denoted by asterisks (*p<0.05; **p<0.01; ***p<0.001).
doi:10.1371/journal.pone.0095023.g004

compared to WT animals at postnatal day 90 in all brain regions examined (Figure 5). These decreases in Cx43, GLAST, and glutamine synthetase in CLN3$^{\Delta ex7/8}$ animals did not result from astrocyte loss, since GFAP expression was significantly elevated in the VC, HPC, and TH (Figure 6) in agreement with previous reports from other laboratories in CLN3 mutant mice [8,20]. This is a key observation, since it reveals the attrition of molecules that regulate glutamate homeostasis in CLN3$^{\Delta ex7/8}$ animals, which likely triggers astrocyte activation in an attempt to rectify this decline. Western blot analysis also revealed significant reductions in Cx43 and glutamine synthetase expression in the S1C, VC, and HPC (Figures S3 and S4); however, some differences were noted in other brain regions compared to confocal microscopy findings. With regard to Cx43, this may be explained by the contributions of other Cx43-positive cell types in brain extracts, including microglia, endothelial cells, ependymal cells, and pericytes [62,63,64,65,66,67] that results in less quantitative precision in Western blots compared to confocal microscopy, although undeniably astrocytes are the major source of Cx43 in the normal CNS. Western blots revealed few differences in Cx30 expression (Figure S5) in agreement with the modest changes detected by immunofluorescence staining. In contrast, Western blotting did not reveal dramatic differences in GLAST expression (Figure S6), which again may be explained by reduced sensitivity compared to immunofluorescence staining. In addition, Western blots are semi-quantitative at best, whereas confocal microscopy is more sensitive at detecting subtle differences in protein levels and immunostaining has been a hallmark method for visualizing differences in glial molecules in JNCL [8,20]. Finally, confocal imaging provides superior precision to reproducibly locate specific brain substructures between different animals (i.e. layers VI-IV of visual cortex) to improve the accuracy of signal quantitation.

CLN3$^{\Delta ex7/8}$ Astrocytes Display Altered Membrane Properties

Electrophysiological recordings of astrocytes in acute brain slices of CLN3$^{\Delta ex7/8}$ and WT mice were made to determine whether any intrinsic defects were evident that could be linked to the observed changes in HC activity or disease progression/severity. No studies to date have evaluated the effects of CLN3 mutation on intrinsic astrocyte properties and our analysis of brain slices is superior to cultured astrocytes where complex interactions with other cell types are lost. In general, CLN3$^{\Delta ex7/8}$ astrocytes were more hyperpolarized compared to WT cells, as revealed by significant changes in RMP in both the S1C (-74.32 ± 0.30, n = 228 vs. -73.31 ± 0.25 mV, n = 216, respectively; $p<0.05$) and HPC (-76.59 ± 0.24, n = 170 vs. -75.73 ± 0.30 mV, n = 138, respectively; $p<0.05$) (Figure 7A). Extrapolation of Gm values revealed consistent reductions in Gm for CLN3$^{\Delta ex7/8}$ astrocytes compared to WT cells both in the S1C and HPC during all three postnatal periods examined, with the exception of day 30 in the latter (Figure 7B and Tables S1 and S2).

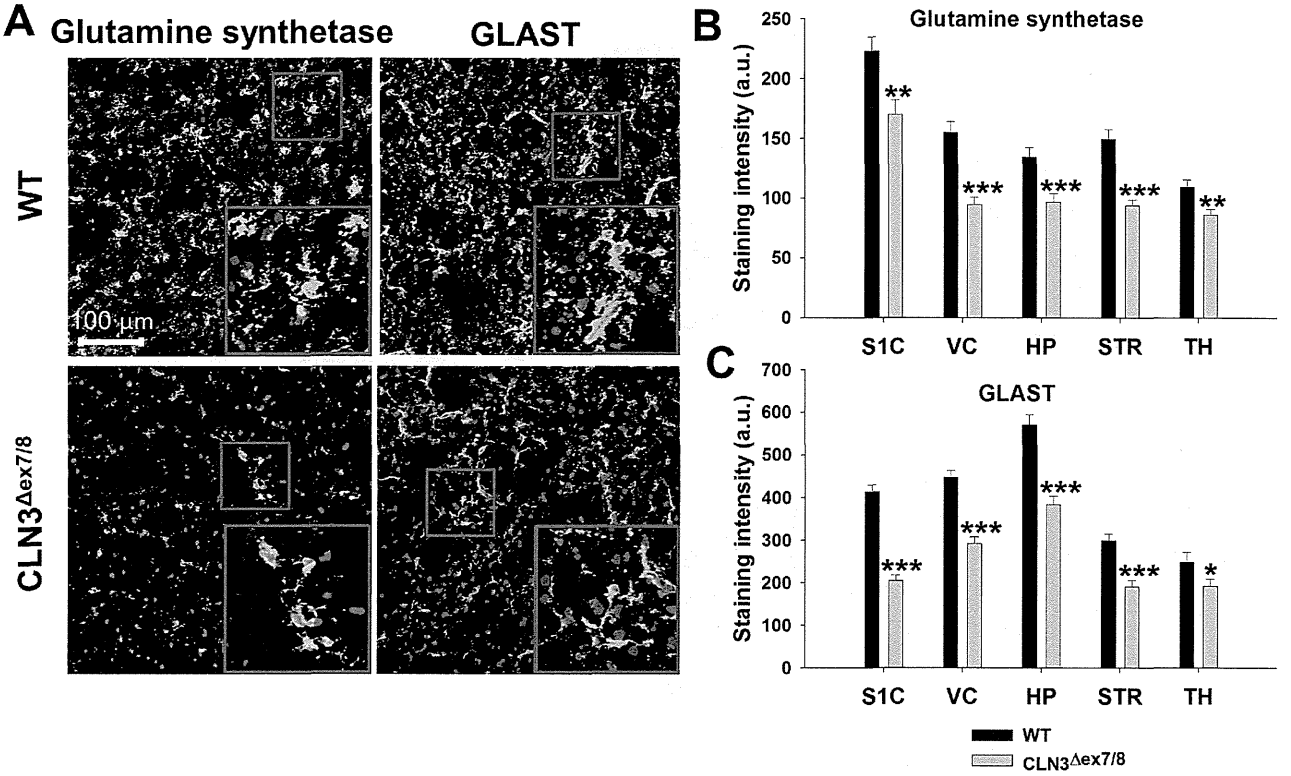

Figure 5. CLN3$^{\Delta ex7/8}$ astrocytes display significant reductions in molecules critical for glutamate homeostasis. Immunofluorescence staining for glutamine synthetase and GLAST was performed on tissue sections from the somatosensory cortex (S1C), visual cortex (VC), hippocampus (HPC), striatum (STR), and thalamus (TH) of wild type (WT) and CLN3$^{\Delta ex7/8}$ mice at postnatal day 90. (A) Representative images depicting glutamine synthetase and GLAST expression in the STR with nuclei depicted by DAPI staining (blue; magnification, 20X; inset 50×50 μm zoom). (B) Glutamine synthetase and (C) GLAST immunoreactivity was quantitated in each brain region (n = 3–4 mice per group; 6 images/region for each animal) with results reported in arbitrary units (a.u.). Significant differences in glutamine synthetase and GLAST staining between WT and CLN3$^{\Delta ex7/8}$ tissues are denoted by asterisks (*$p<0.05$; **$p<0.01$; ***$p<0.001$).
doi:10.1371/journal.pone.0095023.g005

The most dramatic distinction between CLN3$^{\Delta ex7/8}$ and WT astrocytes was in voltage-dependent conductance (Gv). Specifically, CLN3$^{\Delta ex7/8}$ astrocytes revealed significantly decreased Gv compared to WT cells in the S1C (152.3±7.03, n = 292 vs. 187.7±9.56 pA, n = 293, respectively; $p<0.001$) (Figure 7C). Similar decreases in Gv occurred in CLN3$^{\Delta ex7/8}$ astrocytes in the HPC, but were only evident at postnatal day 90 (Figure 7C). In general, decreased Gv in CLN3$^{\Delta ex7/8}$ astrocytes correlates with the observed inhibition of astrocyte HC activity with advancing postnatal age.

The CBX Derivative INI-0602 Attenuates Astrocyte HC Activity in Acute Brain Slices

A recent report described the generation of a novel blood-brain barrier permeable HC inhibitor, INI-0602, which is a derivative of the well-known HC/GJ inhibitor carbenoxolone (CBX) [68]. Treatment with INI-0602 in mouse models of amyotrophic lateral sclerosis and Alzheimer's disease led to significant improvements in motor activity, survival, and cognitive function [68]. Since astrocyte HC activation was increased in CLN3$^{\Delta ex7/8}$ mice at postnatal day 30, we first tested the ability of INI-0602 to inhibit astrocyte HCs in acute brain slices *in vitro* as proof-of-principle. INI-0602 significantly inhibited EtBr uptake in the S1C of both WT and CLN3$^{\Delta ex7/8}$ slices at postnatal day 90 compared with control tissues incubated in ACSF alone (Figure 8A). Importantly, HC activity was similar in CLN3$^{\Delta ex7/8}$ and WT slices bathed in ACSF alone, confirming our earlier findings in the S1C at postnatal day 90 (Figure 3A). INI-0602 also induced changes in astrocyte electrophysiological parameters (Figure 8B) and only WT slices were examined in these experiments to demonstrate drug action on normal cells. Brief INI-0602 application (i.e. 5–10 min) attenuated Gm values in WT astrocytes (365.86±5.96, n = 417 vs. 308.73±4.21 nS, n = 417 vs. 331.48±4.37, n = 280 for ACSF, INI-0602, and drug washout, respectively; $p<0.05$) followed by a depolarizing inward current (−164.2±28.6 pA; range −30 to −600 pA). Gv was significantly increased during INI-application compared to ASCF alone (256.6±23.4 vs. 183.3±14.0 pA, respectively; $p<0.05$). The parental compound CBX prevented the increase in Gv but not membrane depolarization induced by INI-0602 in WT astrocytes (Figure 8B). Since the effects of INI-0602 on intrinsic astrocyte properties could be washed out, this suggests that INI-0602 exerts rapid and reversible changes in astrocyte membrane properties.

The HC Inhibitor INI-0602 Reduces Lysosomal Ceroid Inclusions, Enhances GJC, and Restores Astrocyte RMP in CLN3$^{\Delta ex7/8}$ Mice

Since astrocyte HC activity was increased in several brain regions of CLN3$^{\Delta ex7/8}$ mice at postnatal day 30 and could be blocked by INI-0602 in acute brain slices *in vitro*, we next treated CLN3$^{\Delta ex7/8}$ and WT mice with INI-0602 for a one month period, spanning from postnatal day 30 to 60, to examine its impact on

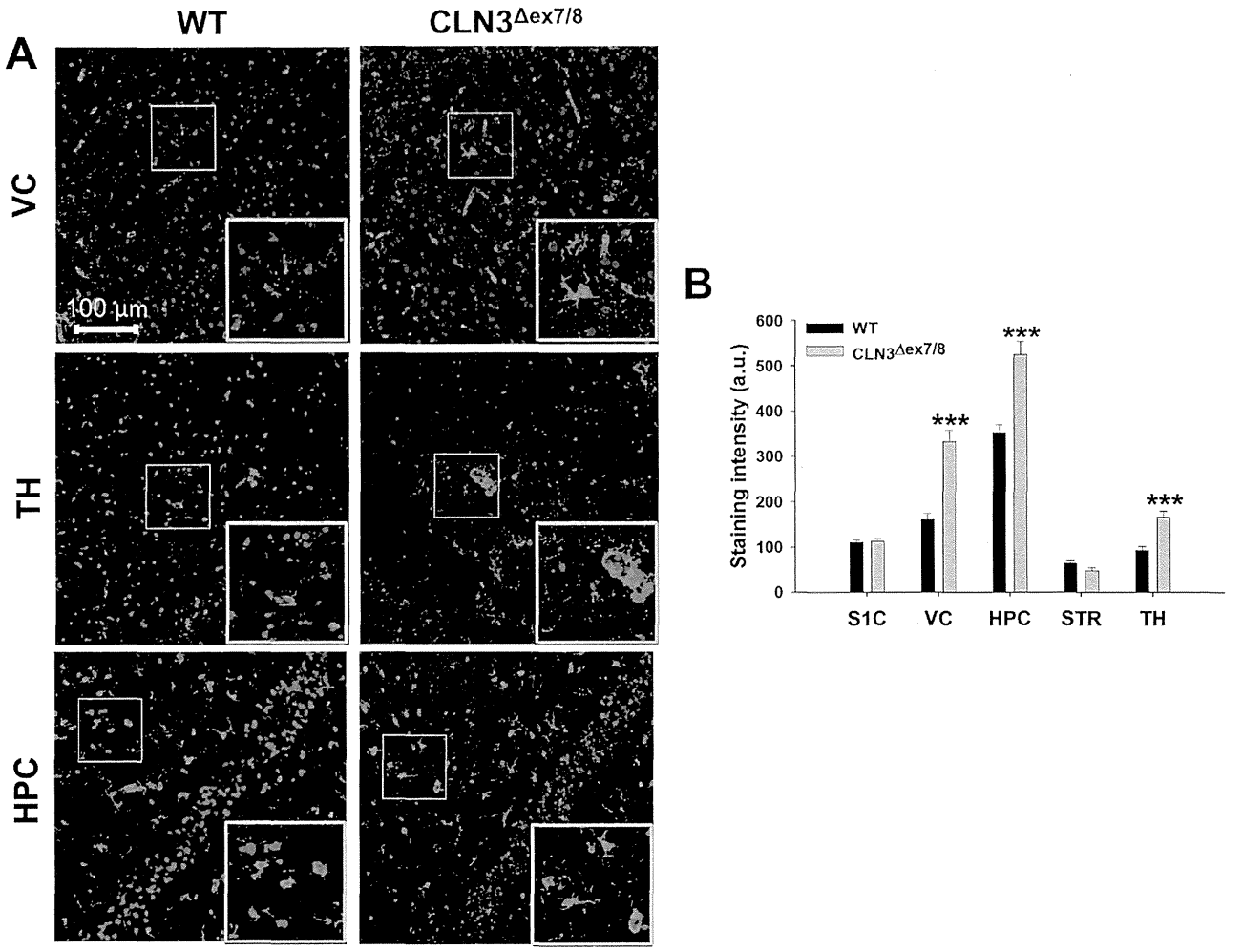

Figure 6. GFAP expression is significantly increased in select brain regions of CLN3$^{\Delta ex7/8}$ mice. Immunofluorescence staining for GFAP was performed on tissue sections from the somatosensory cortex (S1C), visual cortex (VC), hippocampus (HPC), striatum (STR), and thalamus (TH) of wild type (WT) and CLN3$^{\Delta ex7/8}$ mice at postnatal day 90. (A) Representative images depicting GFAP expression in the VC, TH, and HPC with nuclei depicted by DAPI staining (blue; magnification, 20X; inset 50×50 μm zoom). (B) GFAP immunoreactivity was quantitated in each brain region (n = 3–4 mice per group; 6 images/region for each animal) with results reported in arbitrary units (a.u.). Significant differences in GFAP staining between WT and CLN3$^{\Delta ex7/8}$ tissues are denoted by asterisks (***$p<0.001$).
doi:10.1371/journal.pone.0095023.g006

disease parameters. Strikingly, a one month treatment period of CLN3$^{\Delta ex7/8}$ mice with INI-0602 significantly decreased lysosomal ceroid inclusions in three brain regions with the most pronounced accumulation, namely the S1C, VC, and TH compared to CLN3$^{\Delta ex7/8}$ mice receiving PBS (Figure 9A and B).

To determine whether *in vivo* INI-0602 administration had any effects on astrocyte HC/GJ activity, we examined both parameters in acute brain slices recovered from CLN3$^{\Delta ex7/8}$ and WT mice treated with INI-0602 for a one month period. Astrocyte GJC was significantly increased in both CLN3$^{\Delta ex7/8}$ (INI-0602:71.9±3.5, n = 32 vs. PBS: 57.9±3.0 cells, n = 31, $p<0.01$) and WT mice (INI-0602:73.9±3.6, n = 22 vs. PBS: 59.7±5.2 cells, n = 22, $p<0.05$) compared to PBS-treated controls (Figure 9C). Because INI-0602 enhanced GJC, we expected HC activity to be inhibited based on the typical reciprocal relationship reported between these modes of communication in several CNS models [41,42]. Although astrocyte HC opening was significantly elevated in the S1C, VC, HPC, and STR of CLN3$^{\Delta ex7/8}$ mice compared to WT animals, a one month dosing interval with INI-0602 did not reduce HC activity to WT levels (Figure S7). Of note, in these experiments, astrocyte HC activity was significantly increased in CLN3$^{\Delta ex7/8}$ mice at postnatal day 60 in all brain regions examined except the TH, which was not observed in earlier studies (Figure 3A). This may reflect a stress response in CLN3$^{\Delta ex7/8}$ animals precipitated by repeated i.p. injections during the one month dosing period, since elevated HC activity was also observed in CLN3$^{\Delta ex7/8}$ mice receiving PBS. Collectively, these findings suggest that INI-0602 may exert its beneficial effects by enhancing homeostatic GJC by an unknown mechanism. One possibility is that INI-602 provokes transient astrocyte activation, as revealed by its ability to induce slight membrane depolarization (Figure 8B), which may overcome the progressive decline in astrocyte function suggested by the decreases in glutamine synthetase, GLAST, and Cx43 expression in CLN3$^{\Delta ex7/8}$ mice.

Magnetic resonance (MR) spectroscopy is a non-invasive method used to obtain quantitative metabolic information from living animals in serial longitudinal studies [69,70]. MR spectroscopy-visible metabolites include glutamate, glutamine, N-acetyl

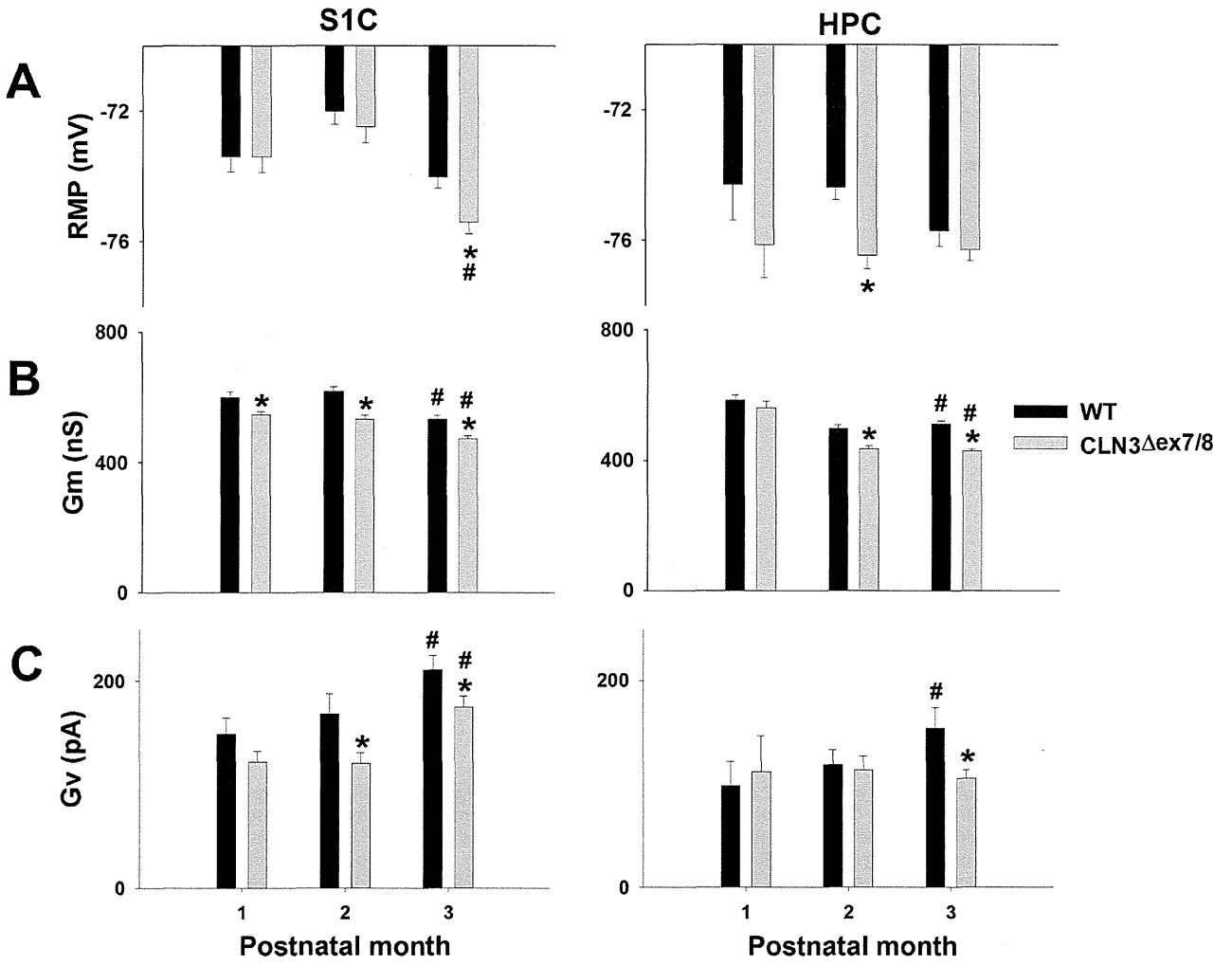

Figure 7. CLN3$^{\Delta ex7/8}$ astrocytes display reductions in membrane potential and conductance. Acute brain slices were prepared from wild type (WT) and CLN3$^{\Delta ex7/8}$ mice at postnatal days 30, 60 and 90, whereupon astrocyte resting membrane potential (RMP; A), resting membrane conductance (Gm; B), and voltage-dependent membrane conductance (Gv; C) were measured in the somatosensory cortex (S1C) and hippocampus (HPC) using whole-cell patch clamp recordings. Significant differences between WT and CLN3$^{\Delta ex7/8}$ astrocytes are denoted by asterisks (*$p<0.05$), whereas changes between values at postnatal days 30 versus 60 or 90 are indicated by hatched signs (#, $p<0.05$). Refer to Tables S1 and S2 for statistical values.

doi:10.1371/journal.pone.0095023.g007

aspartate (NAA), choline, creatine, and myo-inositol [71]; however, recent advances in curve fitting methodology allow for the detection of low-level metabolites, including GABA, glucose, glycine, alanine, aspartic acid, and taurine. A prior report using single-voxel MR spectroscopy revealed elevated glutamate concomitant with reduced GABA during JNCL [60]. We confirmed these observations in the HPC of CLN3$^{\Delta ex7/8}$ mice at postnatal day 60, as revealed by a trend towards elevated glutamate coincident with significantly reduced GABA levels compared to WT animals, although the former did not reach statistical significance (Figure 9D). Since INI-0602 significantly increased astrocyte GJC, we examined whether this would translate into improvements in the brain metabolome of CLN3$^{\Delta ex7/8}$ mice. In general, INI-0602 trended towards restoring glutamate and GABA levels in CLN3$^{\Delta ex7/8}$ animals to levels approaching that of WT mice, but again these differences were not statistically significant (Figure 9D). No other changes in the CNS metabolome were observed between CLN3$^{\Delta ex7/8}$ and WT animals at this early postnatal interval (data not shown).

With regard to astrocyte electrophysiological properties, RMP was slightly hyperpolarized in astrocytes from CLN3$^{\Delta ex7/8}$ mice receiving PBS vehicle and returned to baseline values with INI-0602 treatment (Figure 10A). In addition, INI-0602 significantly increased astrocyte Gm in CLN3$^{\Delta ex7/8}$ mice, whereas Gv values were not affected. However, in comparison, the effects of INI-0602 on astrocyte Gm and Gv were more dramatic in WT animals (Figure 10B and C). Specifically, INI-0602 treatment significantly decreased Gm in WT animals compared to PBS-treated mice (517.8 ± 9.1, $n=477$ vs. 448.4 ± 5.0 nS, $n=336$, $p<0.001$; Figure 10B) as well as Gv (194.1 ± 17.7, $n=92$ vs. 127.8 ± 11.0, $n=84$ pA, $p<0.01$; (Figure 10C).

Although prior studies examining long-term dosing of mice with INI-0602 did not reveal any evidence of toxicity [68], blood chemistry profiles were performed to assess the safety profile of INI-0602 in the context of CLN3 mutation. INI-0602 did not alter

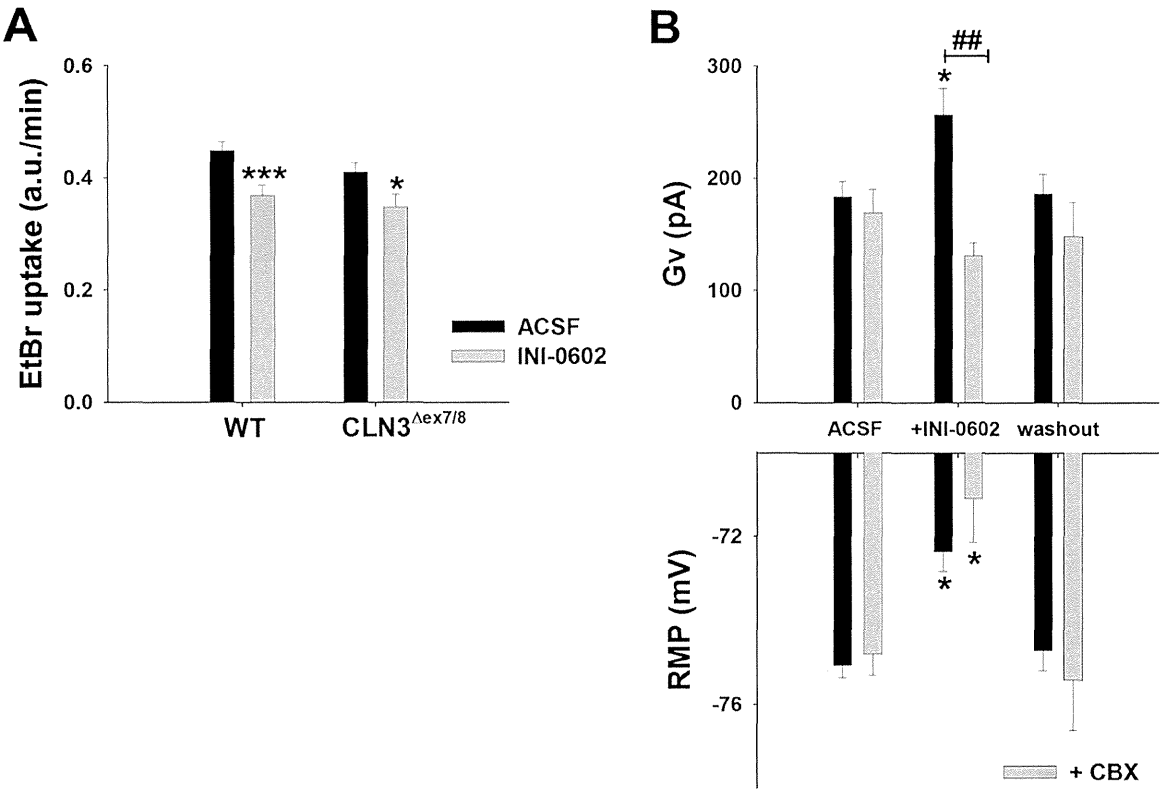

Figure 8. Bath application of INI-0602 inhibits HC activity and alters astrocyte electrophysiological properties. Acute brain slices were prepared from wild type (WT) and CLN3$^{\Delta ex7/8}$ mice at postnatal day 90, whereupon measurements were made in the somatosensory cortex. (A) Direct application of INI-0602 (100 μM) in the bath solution inhibited HC activity of both WT and CLN3$^{\Delta ex7/8}$ astrocytes as measured by the rate of EtBr uptake (presented in arbitrary units (a.u.) per minute). (B) INI-0602 bath application increases voltage-dependent membrane conductance (Gv) of WT astrocytes and evokes membrane depolarization (RMP). Simultaneous bath application of INI-0602 and its parental compound carbenoxolone (CBX; 50 μM) prevented the Gv increase but not RMP depolarization. In (A), significant differences between astrocytes in ACSF alone versus ACSF+INI-0602 are denoted by asterisks (*$p<0.05$; ***$p<0.001$), whereas in (B), significant differences between WT astrocytes bathed in ASCF only versus INI-0602 or INI-0602+ CBX are indicated by asterisks (*$p<0.05$) and alterations between WT astrocytes bathed in INI-0602 versus INI-0602+ CBX are denoted by hatched signs (##, $p<0.01$).
doi:10.1371/journal.pone.0095023.g008

basic blood parameters in either WT or CLN3$^{\Delta ex7/8}$ mice compared to their corresponding PBS controls (Table S3). However, CLN3$^{\Delta ex7/8}$ mice displayed reduced Na^+ and Ca^{2+} compared to WT animals regardless of INI-0602 treatment. No significant weight changes were observed for any of the groups over the one month treatment period (data not shown). Collectively, these results demonstrate that INI-0602 exerts beneficial effects in the JNCL mouse model by reducing lysosomal ceroid inclusions, increasing astrocyte GJC, and normalizing astrocyte RMP without any untoward side effects. The mechanism of action for these findings remains to be fully elucidated; however, the increase in astrocyte GJC observed after a one month treatment period with INI-0602 is an attractive possibility.

Discussion

Reactive astrocytes are a hallmark of JNCL in both the human brain and associated mouse models [8,20], yet little information is available regarding the biological impact of astrocytes on disease pathogenesis. Based on the central role of astrocyte GJC/HC activity in controlling pH and ion balance, vascular control, neuronal activity at the tripartite synapse via glutamate regulation, and metabolic balance, it was envisioned that altered astrocyte function in the context of CLN3 mutation could influence JNCL pathology. CLN3$^{\Delta ex7/8}$ mice displayed increased HC activity at postnatal day 30 in many of the thalamocortical structures where neurons are destined to die at advanced age (i.e. ~ 6 mo. onward), including the TH, STR, and cortical regions [8,72]. Increased HC activity can lead to the dissipation of CNS homeostatic gradients due to the bidirectional communication between the intracellular and extracellular milieus [73]. One such effect emanating from HC opening is glutamate release and although it is tempting to speculate that astrocyte HCs are responsible, in part, for the exaggerated glutamate levels in JNCL reported by other groups [53,59,61], the regulatory mechanisms involved are likely much more complex, since astrocyte HC opening was only transient in CLN3$^{\Delta ex7/8}$ animals. With regard to the brain metabolome, our MR spectroscopy findings revealed significantly decreased GABA in CLN3$^{\Delta ex7/8}$ mice. Although a prior report described elevated glutamate and reduced GABA in CLN3 knockout mice, this analysis was performed using postmortem samples [61]. Importantly, our MR spectroscopy data were collected from living animals, which is more reflective of changes in real time. N-acetyl aspartate (NAA) is a widely used as a surrogate to reflect neuron viability, since it is a neuron-selective metabolite that can be resolved by MR spectroscopy [74]. NAA levels were identical between WT and CLN3$^{\Delta ex7/8}$ mice (data not shown), revealing little evidence of early neuronal pathology in the HPC of

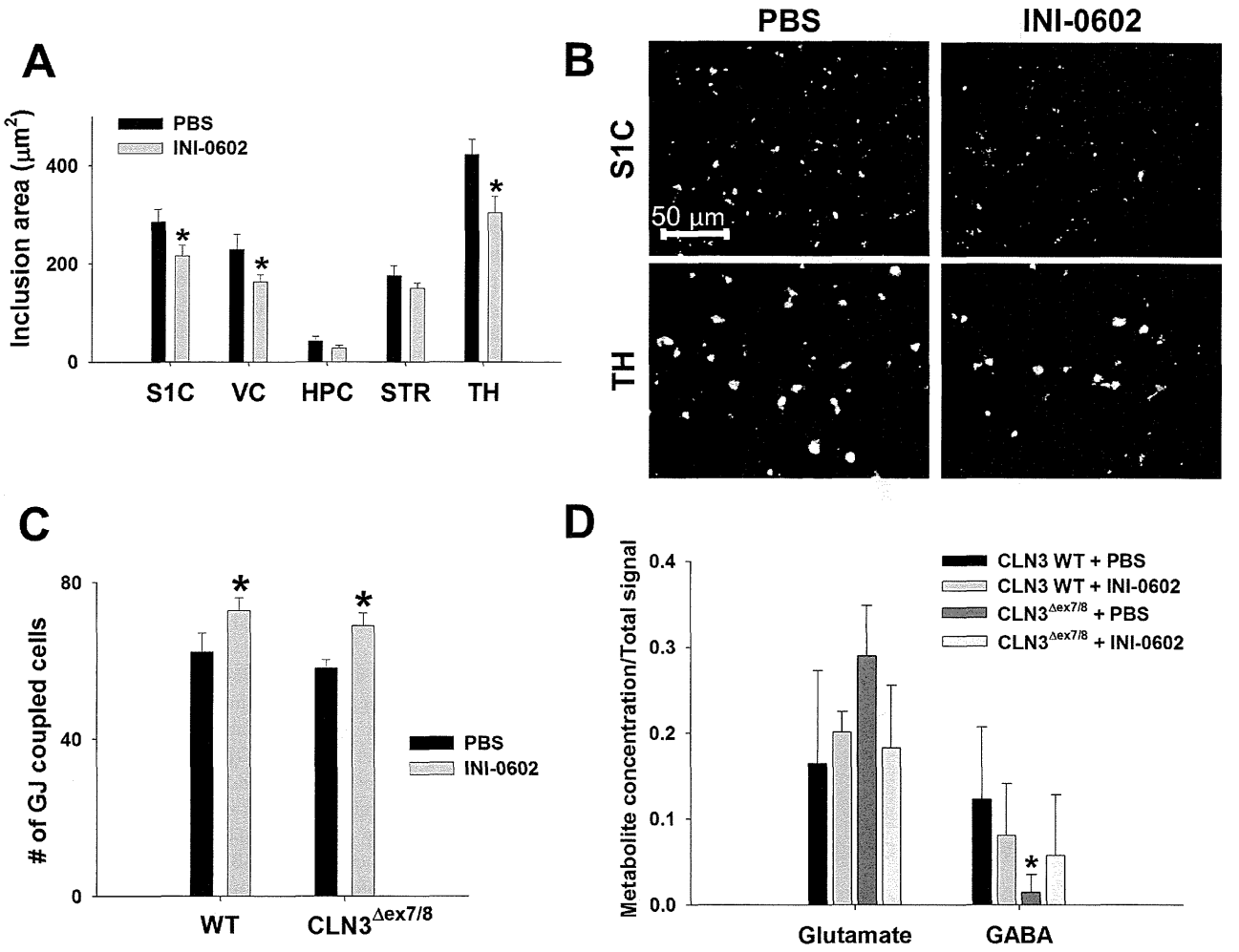

Figure 9. *In vivo* administration of the HC inhibitor INI-0602 reduces ceroid inclusions in CLN3$^{\Delta ex7/8}$ mice and enhances gap junction communication (GJC). CLN3$^{\Delta ex7/8}$ and wild type (WT) mice were treated with INI-0602 (10 mg/kg) or PBS from postnatal day 30 to 60, whereupon measurements were conducted (n = 4–8 mice/group). (A) The area of lysosomal ceroid inclusions in CLN3$^{\Delta ex7/8}$ mice receiving INI-0602 or PBS was quantitated in the somatosensory cortex (S1C), visual cortex (VC), hippocampus (HPC), striatum (STR), and thalamus (TH). (B) Representative images of ceroid inclusions in the S1C or TH of CLN3$^{\Delta ex7/8}$ mice treated with PBS or INI-0602. (C) The number of gap junction (GJ) coupled astrocytes was evaluated in the S1C by monitoring passage of the GJ permeable dye AlexaFluor 350 (n = 21 and 24 cells for PBS- vs. INI-0602-treated WT mice, respectively; n = 36 and 39 cells for PBS- vs. INI-0602-treated CLN3$^{\Delta ex7/8}$ mice, respectively). (D) Glutamate and GABA concentrations in the HPC as measured by magnetic resonance (MR) spectroscopy (n = 4–5 mice/group). Significant differences are indicated by asterisks (*$p<0.05$).
doi:10.1371/journal.pone.0095023.g009

CLN3$^{\Delta ex7/8}$ animals. This was not unexpected because neuronal loss has not been reported to occur until months 6–8 in CLN3$^{\Delta ex7/8}$ mice [8,20] and our MR spectroscopy analysis was performed on 2 month-old animals. It is possible that alterations in the brain metabolome are more pronounced in regions that were not examined here; however, the scan time required to obtain high resolution MR data in living mice for accurate spectroscopy is significant (i.e. ~ 1.5–2 h/mouse), which limited our analysis of numerous brain regions in this study. It is highly likely that more robust changes in the brain metabolome of CLN3$^{\Delta ex7/8}$ mice would be evident at advanced ages; however, we elected to examine animals relatively early in the disease process, since our objective was to intervene with a therapeutic approach during acute disease to delay eventual neuronal loss.

An intriguing finding in the current report was that astrocyte HC opening was only transiently increased in CLN3$^{\Delta ex7/8}$ mice at postnatal day 30. Beyond this interval, HC activity was significantly decreased in CLN3$^{\Delta ex7/8}$ animals compared to WT mice, which coincided with reduced membrane conductance and slight membrane hyperpolarization of CLN3$^{\Delta ex7/8}$ astrocytes both in the S1C and HPC (Figure 7). The reason(s) responsible for the progressive decline in CLN3$^{\Delta ex7/8}$ astrocyte activity are not clear; however, our data showing reduced glutamine synthetase and GLAST expression at postnatal day 90 are suggestive of progressive astrocyte dysfunction (Figure 11). These findings were bolstered by the observation that GFAP levels were significantly elevated in CLN3$^{\Delta ex7/8}$ mice, demonstrating selectivity in targeted molecules. Additional investigations into this possibility are necessary; nevertheless, the central role that astrocytes play in CNS maintenance and neuronal survival suggest this is a mechanism worth pursuing. The decrease in glutamine synthetase and GLAST levels in the CLN3$^{\Delta ex7/8}$ brain reported here is intriguing, since glutamate excitotoxicity represents an important mechanism of neuronal loss in JNCL [53,55]. Reduced glutamine